

A DEFINITIVE SURVEY FOR LYMAN LIMIT SYSTEMS AT $Z \sim 3.5$ WITH THE SLOAN DIGITAL SKY SURVEY

J. XAVIER PROCHASKA¹, JOHN M. O’MEARA², GABOR WORSECK¹

Draft version October 22, 2018

ABSTRACT

We perform a semi-automated survey for $\tau_{912} \geq 2$ Lyman Limit systems (LLSs) in quasar spectra from the Sloan Digital Sky Survey, Data Release 7. From a starting sample of 2473 quasars with $z_{\text{em}} = 3.6 - 4.4$, we analyze 469 spectra meeting strict selection criteria for a total redshift path $\Delta z = 93.8$ and identify 192 intervening systems at $z_{\text{LLS}} \geq 3.3$. The incidence of $\tau_{912} \geq 2$ LLSs per unit redshift, $\ell_{\tau \geq 2}(z)$, is well described by a single-power law at these redshifts: $\ell_{\tau \geq 2}(z) = C_{\text{LLS}}[(1+z)/(1+z_*)]^{\gamma_{\text{LLS}}}$, with $z_* \equiv 3.7$, $C_{\text{LLS}} = 1.9 \pm 0.2$, and $\gamma_{\text{LLS}} = 5.2 \pm 1.5$ (68% c.l.). These values are systematically lower than previous estimates (especially at $z < 4$) but are consistent with recent measurements of the mean free path to ionizing radiation. Extrapolations of this power-law to $z = 0$ are inconsistent with previous estimations of $\ell(z)$ at $z < 1$ and suggest a break at $z \approx 2$, similar to that observed for the Ly α forest. Our results also indicate that the systems giving rise to LLS absorption decrease by $\approx 50\%$ in comoving number density and/or physical size from $z = 4$ to 3.3, perhaps due to an enhanced extragalactic ultraviolet background. The observations place an integral constraint on the H I frequency distribution $f(N_{\text{HI}}, X)$ and indicate that the power-law slope $\beta \equiv d \ln f(N_{\text{HI}}, X) / d \ln N_{\text{HI}}$ is likely shallower than $\beta = -1$ at $N_{\text{HI}} \approx 10^{18} \text{ cm}^{-2}$. Including other constraints on $f(N_{\text{HI}}, X)$ from the literature, we infer that β is steeper than $\beta = -1.7$ at $N_{\text{HI}} \approx 10^{15} \text{ cm}^{-2}$, implying at least two inflections in $f(N_{\text{HI}}, X)$. We also perform a survey for proximate LLSs (PLLSs) and find that $\ell_{\text{PLLS}}(z)$ is systematically lower ($\approx 25\%$) than intervening systems. Finally, we estimate that systematic effects impose an uncertainty of 10 – 20% in the $\ell(z)$ measurements; these effects may limit the precision of all future surveys.

Subject headings: absorption lines – intergalactic medium – Lyman limit systems – SDSS

1. INTRODUCTION

Studies of hydrogen absorption in the lines of sight towards distant quasars have served to both define, and in recent years bring precision to, our cosmological models. The low density, highly ionized Lyman- α forest lines (a.k.a. the intergalactic medium, IGM), with H I column densities $N_{\text{HI}} < 10^{17.2} \text{ cm}^{-2}$, have through their aggregate statistical properties (e.g. their flux power spectrum, mean flux, and column density distributions) constrained cosmological parameters such as the primordial power spectrum and the baryonic mass density and astrophysical parameters like the amplitude of the ionizing background (e.g. Rauch 1998; Croft et al. 2002; McDonald et al. 2005; Tytler et al. 2004; Faucher-Giguère et al. 2008b). The high-density, predominantly neutral damped Ly α systems (DLAs), with $N_{\text{HI}} \geq 10^{20.3} \text{ cm}^{-2}$, trace the gas which forms stars, and likely represent the progenitors of modern-day galaxies (e.g. Wolfe et al. 1995, 2005; Prochaska & Wolfe 2009).

The majority of Lyman- α forest lines and the DLAs have, through analysis of their Ly α lines, precisely measured N_{HI} values that permit detailed study of their physical properties (e.g. metallicity). For systems with intermediate N_{HI} values ($\approx 10^{18} \text{ cm}^{-2}$), however, Ly α and most of the Lyman series lines lie on the flat portion of the curve-of-growth making the N_{HI} value difficult to

constrain. On the other hand, these systems are optically thick to ionizing radiation and impose a readily identified signature in a quasar spectrum at the Lyman limit. These so-called Lyman limit systems (LLSs), currently the least-well studied of H I absorption systems at high redshift, are the focus of this manuscript.

Historically, the LLSs were among the first class of quasar absorption line (QAL) systems to be surveyed (Tytler 1982). This is because their spectral signature is obvious in low-resolution, low S/N spectra. The principal challenge is that the Lyman limit occurs redward of the atmospheric cutoff only for systems with redshifts $z > 2.6$. For lower redshifts, one requires spectrometers on space-borne ultraviolet satellites. By the mid 1990’s, samples of several tens of LLSs were generated spanning redshifts $0 < z < 4$ (Sargent et al. 1989; Lanzetta 1991; Storrie-Lombardi et al. 1994; Stengler-Larrea et al. 1995). These results were derived from heterogeneous sets of quasars discovered from a combination of color-selection, radio detection, and slitless spectroscopic surveys. The spectra, too, were acquired with a diverse set of instrumentation and therefore varying S/N and spectral resolution mitigating differing sensitivity to the precise optical depth at the Lyman limit. Although the results were not fully consistent with one another, the general picture that resulted was a rapidly evolving population of absorption systems reasonably described by a $(1+z)^{1.5}$ power-law.

Cosmologically, the LLSs contribute much if not most of the universe’s opacity to ionizing radiation. And, until recently, the observed incidence of the LLS provided the only direct means of estimating the mean free path $\lambda_{\text{mfp}}^{912}$

¹ Department of Astronomy and Astrophysics, UCO/Lick Observatory, University of California, 1156 High Street, Santa Cruz, CA 95064

² Department of Chemistry and Physics, Saint Michael’s College. One Winooski Park, Colchester, VT 05439

at any redshift (e.g. Meiksin & Madau 1993; Madau et al. 1999; Faucher-Giguère et al. 2008a). In a companion paper (Prochaska et al. 2009, ; hereafter PWO09), we have presented a new technique to measure $\lambda_{\text{mfp}}^{912}$ that circumvents any knowledge of the LLSs. A more precise census of the LLSs will serve as a consistency check for this $\lambda_{\text{mfp}}^{912}$ calculation, but is unlikely to ever again be a competitive approach. Instead, the incidence of LLS can be used in combination with estimates of $\lambda_{\text{mfp}}^{912}$ to assess the N_{HI} frequency distribution for gas with $N_{\text{HI}} \approx 10^{16-18} \text{ cm}^{-2}$, a regime that is very difficult to explore by studying individual absorption systems. Surveys of the LLSs are also likely to place tight constraints on $z \sim 3$ cosmological simulations that include radiative transfer.

Physically, the nature of systems that give rise to a LLS remains an open question. The systems with the largest N_{HI} values (i.e. $N_{\text{HI}} \geq 10^{19} \text{ cm}^{-2}$, the so-called the super-LLS or SLLS and DLAs) are likely associated with the interstellar medium and outer regions of high z galaxies. These high N_{HI} systems, however, are only a subset of the LLS population. Unfortunately, a proper modeling of the LLSs almost certainly requires careful modeling of radiative transfer in cosmological simulations which has thus far been beyond the scope of modern computations in cosmological simulations. Indeed, the few studies to date have tended to severely underestimate the incidence of LLS (Katz et al. 1996; Gardner et al. 2001, but see Kohler & Gnedin 2007). In recent simulations of high z galaxy formation, however, theorists have placed great attention on ‘streams’ of cold gas that carry fresh material from the IGM to star-forming galaxies (Kereš et al. 2005; Dekel et al. 2009). These cold streams have relatively large hydrogen surface densities ($N_{\text{H}} \sim 10^{20} \text{ cm}^{-2}$) and could therefore produce Lyman limit absorption provided the material has a non-negligible neutral fraction. Consequently, an accurate census of the LLSs with redshift may directly constrain the nature and prevalence of cold streams in the young universe.

A final, yet perhaps most important, motivation for studying the LLSs is that these systems may dominate the census of metals at all epochs. The majority of LLSs are metal-bearing, showing metal-line transitions of common low and high-ions (e.g. Prochaska 1999; Prochter et al. 2009). Because the estimated ionization corrections for LLSs with $N_{\text{HI}} \approx 10^{18} \text{ cm}^{-2}$ is large, observations of ions in an LLS likely track only a trace amount of the metals actually present in the gas. Lyman limit systems may show a wider spread in their ionization and metal content relative to the IGM or DLA, further emphasizing the need for a robust LLS survey.

In this paper, we survey the homogeneous dataset of quasar spectra from the Sloan Digital Sky Survey (SDSS), using all 7 public data releases. Our observational analysis aims to produce the most precise measurement of the LLS incidence paying careful attention to systematic biases. The wavelength coverage and data quality of the SDSS quasar spectra focus the survey at $z \approx 3.5$. Future work will depend on follow-up observations of well-defined quasar samples at other wavelengths.

The paper is organized as follows. In § 2, we present a set of LLS definitions used throughout the manuscript.

The selection criteria and data quality of quasars from the SDSS database are described in § 3. The procedure to model the absorbed quasar continuum is presented in § 4 and the search and characterization of LLSs is detailed in § 5. The criteria used to measure the survey path are described in § 6 and an assessment of systematic error and bias from analysis of mock spectra is provided in § 7. § 8 describes the principal results and the implications for the IGM and cosmology are discussed in § 9. Finally, § 10 presents a summary of the main findings. Throughout the paper, we adopt a Λ CDM cosmology with $H_0 = 72 h_{72} \text{ km s}^{-1} \text{ Mpc}^{-1}$, $\Omega_{\text{m}} = 0.3$, and $\Omega_{\Lambda} = 0.7$ and report proper lengths unless otherwise indicated.

2. LYMAN LIMIT SYSTEM DEFINITIONS

The photon cross-section of a hydrogen atom at energies above the Lyman limit may be approximated by:

$$\sigma_{\text{LL}}(\nu \geq \nu_{912}) \approx 6.35 \times 10^{-18} \left(\frac{\nu}{\nu_{912}} \right)^{-3} \text{ cm}^2, \quad (1)$$

with

$$\nu_{912} = E_{912}/h = c/\lambda_{912}, \quad (2)$$

and $E_{912} = 1 \text{ Ryd}$. Specifically, $\nu_{912} = 3.29 \times 10^{15} \text{ Hz}$ and $\lambda_{912} = 911.7641 \text{ \AA}$. This implies an optical depth at wavelengths $\lambda \leq \lambda_{912}$,

$$\tau_{\text{LL}}(\lambda \leq \lambda_{912}) \approx \frac{N_{\text{HI}}}{10^{17.2} \text{ cm}^{-2}} \left(\frac{\lambda}{\lambda_{912}} \right)^{-3}, \quad (3)$$

where N_{HI} is the H I column density. For a gas ‘cloud’ intersecting a background source with intrinsic flux $F_{\text{int}}(\lambda)$, the observed flux $F_{\text{obs}}(\lambda)$ blueward of the Lyman limit is

$$F_{\text{obs}}(\lambda \leq \lambda_{912}) = F_{\text{int}}(\lambda) \exp[-\tau_{\text{LL}}(\lambda)] \quad (4)$$

In what follows, we define a ‘standard’ Lyman limit system to be one where the optical depth at λ_{912} is $\tau_{912} \geq 2$, i.e. $N_{\text{HI}} \geq 10^{17.5} \text{ cm}^{-2}$. We refer to these systems as the $\tau_{912} \geq 2$ LLS. This corresponds to greater than 85% attenuation of an incident ionizing radiation field at $\nu = \nu_{912}$. By this definition, the class of LLS includes systems with $10^{20.3} \text{ cm}^{-2} \geq N_{\text{HI}} \geq 10^{19} \text{ cm}^{-2}$ (the so-called super-LLS or sub-DLAs, hereafter referred to as SLLS; e.g. O’Meara et al. 2007) and systems with $N_{\text{HI}} \geq 10^{20.3} \text{ cm}^{-2}$ (the damped Ly α systems, DLAs; e.g. Wolfe et al. 2005). In a few cases, we will distinguish between these ‘strong’ LLSs from those with lower N_{HI} , referring to the latter as $\tau_{912} \lesssim 10$ LLS. We also note that our $\tau_{912} \geq 2$ definition for a LLS differs from other works which adopted $\tau_{912} \geq 1$ or $\tau_{912} \geq 1.5$. These are all observationally-driven, not physically-motivated definitions.

Observationally, the absorption of a background source by a $\tau_{912} \geq 2$ LLS is readily apparent, even in low S/N spectra. We define absorbers with $\tau_{912} < 2$ (i.e. $N_{\text{HI}} < 10^{17.5} \text{ cm}^{-2}$) as the partial Lyman limit systems (pLLSs). To survey these systems, one requires higher quality spectra or an alternate approach to the analysis.

We define the redshift of an LLS as

$$z_{\text{LLS}} \equiv \frac{\lambda_{912}^{\text{LLS}}}{\lambda_{912}} - 1 \quad (5)$$

where $\lambda_{912}^{\text{LLS}}$ marks the observed onset of LL absorption. In practice, this is often estimated from strong Lyman series lines (e.g. Ly α , Ly β) that accompany the Lyman limit opacity.

We define the sub-set of LLSs that occur within 3000 km s $^{-1}$ of the emission redshift of the background source as proximate LLSs (PLLSs). We separate the analysis of these systems from the rest to investigate changes in the incidence of optically thick gas near high z quasars due to, e.g. the quasar’s radiation field and local environment.

Finally, we define the observable $\ell_{\tau \geq 2}(z)$ as the average number of $\tau_{912} \geq 2$ LLS detected per unit redshift at a given redshift. In the previous literature, this quantity is also expressed as $n(z)$, dN/dz , and dn/dz . For comparison with previous results in the literature, we also consider $\ell_{\tau \geq 1}(z)$, the number of $\tau_{912} \geq 1$ LLSs detected per unit redshift. We also attempt to separate the contributions to $\ell_{\tau \geq 2}(z)$ from SLLSs $\ell_{\text{SLLS}}(z)$, DLAs $\ell_{\text{DLA}}(z)$, and attribute the remainder to the LLSs with $10^{17.5} \leq N_{\text{HI}} < 10^{19} \text{ cm}^{-2}$, $\ell_{\text{LLS}}(z)$.

3. SDSS QUASAR SAMPLE AND SPECTROSCOPY

One of the primary objectives of the Sloan Digital Sky Survey (SDSS) was to discover $\sim 100,000$ new quasars across the northern sky (York et al. 2000). The strategy of the SDSS team to achieve this ambitious goal was a four-fold process: (i) obtain deep, multi-band images across a large area of the sky; (ii) select quasar candidates by demanding a point-like, point-spread-function and imposing color criteria that separate the candidates from the Galactic stellar locus; (iii) obtain follow-up spectra for a magnitude-limited sample with a fiber-fed spectrograph. The details of target selection and quasar completeness with redshift is described at length in a series of SDSS papers (e.g. Richards et al. 2002), but see Worseck & Prochaska (2009) for a new and more accurate analysis; and (iv) automatically identify quasars and estimate their redshifts (z_{em}) through template fitting to the optical spectroscopy.

Of these steps, the second has the greatest impact on a survey for high z Lyman limit systems. The key issue for our survey is whether the presence of an intervening LLS biases the targeting of the background quasar for follow-up spectroscopy. In effect, a high z LLS severely ‘reddens’ the quasar at the bluest optical wavelengths of the SDSS imaging. With this effect in mind, the SDSS team imposed cuts on the ($u - g$) color which better separated the quasar locus in color space from the stellar locus. The net effect, however, is to bias the spectroscopic follow-up against quasar sightlines *without* a foreground LLS (PWO09). Our analysis indicates an important bias for quasars with $z_{\text{em}} < 3.6$. For this reason, we limit the statistical analysis to quasars with $z_{\text{em}} \geq 3.6$, but we also explore the bias by considering the incidence of LLSs toward quasars with $z_{\text{em}} = 3.4 - 3.6$.

The quasar spectra analyzed in this paper were taken from the Sloan Digital Sky Survey, Data Release 7 (Abazajian et al. 2009). We retrieved the ‘best’ 1D spectrum for every source flagged as a QSO or HIZ_QSO. This

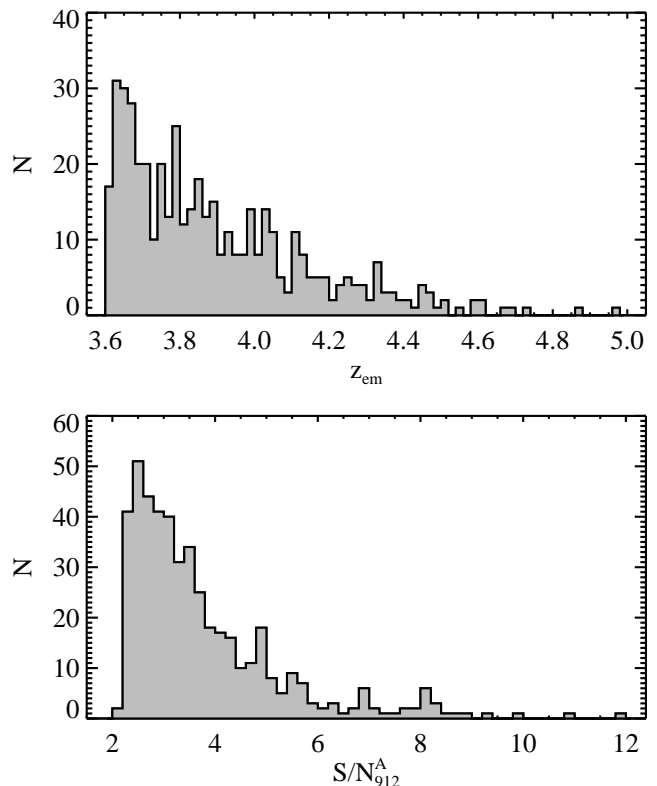


FIG. 1.— Histograms of (top) the emission redshifts z_{em} for the quasars comprising our survey and (bottom) the measurements of S/N_{912}^A , the signal-to-noise of the absorbed continuum at the Lyman limit of each quasar. The sample is restricted to $S/N_{912}^A \geq 2$.

totalled 102,418 unique spectra³. The SDSS survey employs a fiber-fed, dual-camera spectrometer that provides continuous wavelength coverage from $\lambda \approx 3800 - 9200 \text{ \AA}$ at a spectral resolution of $\text{FWHM} \approx 150 \text{ km s}^{-1}$. The SDSS team employs a custom, data-reduction pipeline that performs sky subtraction using empirical measurements from fibers placed to avoid objects detected in the SDSS images. The majority of data suffer from excessive sky noise at long wavelengths ($\lambda > 8000 \text{ \AA}$) and the instrument throughput and atmospheric absorption limits the sensitivity at the shortest wavelengths ($\lambda < 4200 \text{ \AA}$).

A survey for H I Lyman limit absorption in quasar spectra involves two principle steps. First, one must assess the flux at wavelengths near the Lyman limit in the quasar’s rest-frame, $\lambda \lesssim \lambda_{912}(1 + z_{\text{em}})$. We discuss our procedure for this step in the following section. The second step is to estimate the flux at wavelengths blueward of LLS candidates. There are several characteristics of the SDSS spectroscopy which negatively affect this estimate. A generic concern is the poorer instrument response at the bluest wavelengths. At the bluest wavelengths, many of the spectra exhibit a very low signal-to-noise ratio and yield flux estimates consistent with zero, even without an intervening LLS. Therefore, we have limited our survey to redshifts $z_{\text{LLS}} \geq 3.3$ corresponding to

³ The SDSS spectra were processed through our automated algorithms for finding absorption-line features and damped Ly α candidates (Prochaska et al. 2005; Herbert-Fort et al. 2006). Approximately 10 of the spectra failed to be processed (primarily because the SDSS-reported emission redshift is erroneous) and were removed from any subsequent analysis.

$\lambda > 3920\text{\AA}$. In practice, we restrict the quasar sample to objects with $z_{\text{em}} \geq 3.6$ and perform a search for LLSs at all redshifts, but then only analyze absorption systems with $z_{\text{LLS}} \geq 3.3$. We also limit the survey to quasars with $z_{\text{em}} \leq 5$ because the SDSS spectra of higher redshift objects are generally too low S/N to permit a robust analysis. Figure 1a presents histograms of the emission redshifts for the statistical sample and the signal-to-noise of the absorbed continuum at the Lyman limit (S/N_{912}^A ; see below for the definition).

Another difficulty with the SDSS spectra at blue wavelengths is that the two-dimensional spectra of faint sources may be improperly traced. On occasion, the 1D extractions include flux from a neighboring object and yield a systematic overestimate of the flux. This effect reduces the estimated opacity for a LLS. Another issue, especially with a fiber-fed spectrometer, is that the sky model is estimated from nearby fibers that are intentionally placed on ‘object-free’ regions of the sky. Although the SDSS project has worked carefully to mitigate the effects of variable fiber efficiency, significant misestimates of the sky are known to occur. We have identified tens of objects where the extracted flux is significantly negative, indicating an overestimate in the sky model. This may convert a partial LLS (with $\tau_{912} < 1$) into a $\tau_{912} \geq 2$ LLS. By a similar token, a proper $\tau_{912} \geq 2$ LLS may appear as a pLLS if the sky is underestimated. We proceed under the expectation that this effect is nearly random, i.e. for every underestimate of the sky there is a corresponding overestimate, but this has not been rigorously established. The SDSS fibers are sufficiently wide (diameter of $3''$) that they will occasionally include flux from a projected neighbor. These coincident objects may be much fainter than the quasar at redder wavelengths, but they could contribute all of the flux blueward of a strong LLS and lead to an underestimate of the LL opacity⁴.

4. THE ABSORBED QUASAR CONTINUUM

Absent any other sources of opacity, one can trivially estimate τ_{912} from the quasar spectrum through measurements of the flux both redward and blueward of the observed Lyman limit (Equation 4). In practice, however, the quasar flux is also attenuated by line opacity from the so-called Ly α forest (a.k.a., the intergalactic medium; IGM). For example, consider a Lyman limit system at $z_{\text{LLS}} = 3.5$ intervening a $z_{\text{em}} = 4$ quasar. The LLS attenuates the quasar flux blueward of $\lambda_{912}^{\text{LLS}} = 4103\text{\AA}$. At this wavelength, the quasar spectrum recorded on Earth will also include opacity from the Ly α forest at $z_{\text{Ly}\alpha} = (1 + z_{\text{LLS}})(\lambda_{912}/\lambda_{\text{Ly}\alpha}) - 1$, Ly β absorption from the IGM at $z_{\text{Ly}\beta} = (1 + z_{\text{LLS}})(\lambda_{912}/\lambda_{\text{Ly}\beta}) - 1$, etc. It is necessary, therefore, to account for these additional sources of opacity when estimating τ_{912} .

We can express the observed (rest-frame) quasar flux F_{obs} in terms of the intrinsic flux (just) redward of the Lyman limit F_{int} as

$$F_{\text{obs}}(\lambda \gtrsim \lambda_{912}) = F_{\text{int}} \exp[-\tau_{\text{IGM}}(\lambda)] \quad , \quad (6)$$

⁴ An amusing (and plausible) systematic effect related to this is contamination by the light reflected from terrestrial satellites crossing the night sky. Even a brief ‘exposure’ through the $3''$ fiber could dominate the flux at the bluest wavelengths, although this should generally be mitigated by the fact that the SDSS team acquires 3 unique exposures per target.

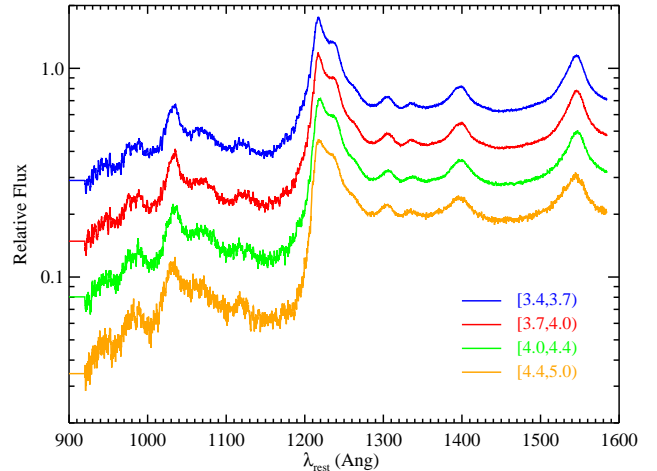


FIG. 2.— Mean observed quasar spectra from the SDSS-DR3 in redshift intervals from top to bottom of $z = [3.4, 3.7]; [3.7, 4.0]; [4.0, 4.4]$ and $[4.4, 5.0]$. The spectra have been offset by a factor of 1.5 for presentation purposes and the normalization is not physically meaningful. The increasing impact of the Ly α forest is readily apparent at wavelengths $\lambda_{\text{rest}} < 1200\text{\AA}$. At $\lambda_{\text{rest}} < 920\text{\AA}$, we have set the template to a constant value.

where τ_{IGM} is the effective opacity of the IGM from Lyman series line-opacity⁵. The LLS introduces an additional, continuous opacity blueward of the Lyman limit:

$$F_{\text{obs}}(\lambda \leq \lambda_{912}) = F_{\text{int}} \exp[-\tau_{\text{IGM}}(\lambda) - \tau_{\text{LL}}(\lambda)] \quad . \quad (7)$$

A precise estimate of $\tau_{912} = \tau_{\text{LL}}(\lambda_{912})$, therefore, requires an estimation of the absorbed quasar flux not its intrinsic flux. Conveniently, this quantity is the observed flux recorded in the spectrum at $\lambda \gtrsim \lambda_{912}$. There are still significant challenges because the IGM opacity is stochastic on both small (individual Lyman lines) and modest scales (many 10\AA) and the intrinsic quasar spectrum (both shape and normalization) varies from source to source. We now describe an automated procedure used to estimate the absorbed continuum from each quasar spectrum.

The traditional method of estimating the quasar continuum is to first identify regions of unabsorbed quasar flux and then to interpolate a continuum level between these regions. For quasars at high redshift, this method is particularly error prone, because at wavelengths below Ly α emission we expect few (and at very high redshift, none) of the pixels to be free of absorption from the IGM. Moreover, this traditional method frequently requires by-hand modification, which is time-intensive and subjective to individual biases. Methods do exist to automatically generate a quasar continuum from emission-line characteristics (e.g. Suzuki 2006), but these are designed to infer the intrinsic quasar spectrum not the IGM-absorbed continuum.

Our approach is to match a template model of the average absorbed continuum to each spectrum, allowing for a large-scale tilt (i.e. a unique underlying power-law slope) and arbitrary normalization. We emphasize that this approach is not intended to recover the intrinsic spectral energy distribution of the quasars. Our scientific inter-

⁵ In the following, we do not explicitly derive the opacity from metals in the IGM, but these may be considered included in τ_{IGM} .

TABLE 1
SDSS-DR7 QUASAR SAMPLE

Plate	MJD	FiberID	Object Name	z_{em}	flg^a	A^b	B^b	Scale ^c	S/N_{912}^A . ^d
650	52143	111	J000238.41−101149.8	3.938	0	2.60	−0.29	1.11	0.9
750	52235	608	J000300.34+160027.7	3.698	0	16.35	−3.54	1.00	1.5
650	52143	48	J000303.34−105150.6	3.646	0	46.77	−11.08	0.96	2.0
750	52235	36	J000335.21+144743.6	3.484	0	13.96	−3.23	1.12	0.8
751	52251	207	J000536.38+135949.4	3.686	0	9.96	−2.00	1.00	1.1
751	52251	562	J000730.82+160732.5	3.501	0	7.35	−1.26	1.15	1.2
651	52141	534	J001001.02−090519.1	3.720	2				
751	52251	39	J001115.23+144601.8	4.967	0	80.36	−18.34	1.00	3.0
752	52251	378	J001134.52+155137.3	4.325	0	15.67	−3.60	1.00	1.1
752	52251	204	J001328.21+135828.0	3.575	0	16.28	−2.75	1.07	2.5
752	52251	5	J001747.90+141015.7	3.955	0	21.69	−5.06	0.92	1.0
753	52233	310	J001813.88+142455.6	4.235	0	22.74	−5.04	1.00	1.7
753	52233	291	J001820.71+141851.5	3.936	0	70.03	−16.86	1.32	3.6
753	52233	391	J001918.43+150611.3	4.134	0	1.91	0.13	1.13	1.2
390	51900	271	J001950.05−004040.7	4.327	0	21.55	−4.96	0.89	1.9

NOTE. — [The complete version of this table is in the electronic edition of the Journal. The printed edition contains only a sample.]

^aFlag indicating: 0=Normal; 1=Not at SDSS reported redshift and/or not a quasar (excluded); 2=Too low S/N for evaluation (excluded); 3=Strong BAL (excluded)

^bAbsorbed continuum fitting parameters of the form: $C = A + B \log_{10}(\lambda/\text{\AA})$. We caution the reader that these models are not meant to describe the intrinsic spectral energy distributions of the quasars (see the text).

^cAdditional scaling factor imposed by the authors on the best-fit absorbed quasar continuum.

^dEstimate of the signal-to-noise for the absorbed quasar continuum at $\lambda = \lambda_{912}(1 + z_{\text{em}})$.

est, in this manuscript, is to model the absorbed continuum of a quasar near its Lyman limit with the fewest number of parameters. Indeed, for some quasars we derive power-law slopes that are likely unphysical due to the stochastic nature of IGM absorption, the non-linear effects of emission lines, intrinsic deviations from a single power-law, and the narrow spectral range considered. We caution against using any of the following results for studies on the physical properties of high z quasars.

Our first step is to derive the templates for the average absorbed quasar continuum. Because the line-density of the IGM and therefore τ_{IGM} increase with redshift, we perform this analysis in small redshift intervals ($\delta z = 0.3$ to 0.6; Figure 2). For every quasar within the redshift interval, we shift the spectrum to the quasar rest-frame using the SDSS reported z_{em} value. Next, we “detilt” the spectrum by removing a power-law shape. This power-law is determined as follows.

We have constructed from the SDSS-DR3 dataset an average template spectrum, archived in XIDL⁶ as “full_SDSS_LLS.fits”. For each individual quasar spectrum, we sample quasar pixels with wavelengths greater than Ly α emission, divide by the template spectrum, and measure the slope of the resulting spectrum. After aligning the spectra in the quasar rest-frame (nearest pixel), we median-combine the data in each redshift interval⁷. The resultant template represents the median intrinsic quasar continuum modulated by the median flux decrement of the IGM. Due to the presence of Lyman limit systems, the quasar templates will not be useful at wavelengths near and below the rest-frame Lyman limit; this portion of the spectrum, however, can be used to constrain the mean free path to ionizing radiation (PWO09). For wavelengths blueward of 920 \AA ,

therefore, we set the template to have the value recorded at 920 \AA . Conveniently, there are no strong emission features in the quasar SED at these wavelengths (e.g. Telfer et al. 2002). The resultant template spectra are shown in Figure 2.

With the templates constructed, a model of the absorbed continuum for each quasar is determined as follows. First, we shift the observed quasar spectrum to the rest-frame and divide by the appropriate template spectrum (i.e. according to z_{em}). Second, we sample the quasar in the wavelength range $950\text{\AA} < \lambda < 1800\text{\AA}$ and fit a power-law ($p(\lambda) = A + B \log[\lambda/\text{\AA}]$) to the observed flux, weighting by the inverse variance array. The emission lines in this spectral range may bias the fit, but we do review and modify these fits (see below). The product of this power-law with the template, when shifted to the observed frame, provides our model for the absorbed quasar continuum. The power-law parameters derived in this fashion are listed in Table 1. Sample fits are shown in Figure 3. With these models, we can calculate the ratio of the absorbed continuum to the 1σ -error array each quasar’s Lyman limit, which we denote as S/N_{912}^A . Figure 1b shows the distribution of S/N_{912}^A values for the statistical survey.

5. LYMAN LIMIT SYSTEM SEARCH AND CHARACTERIZATION

In the following, we parameterize a LLS by two quantities: (1) its absorption redshift z_{LLS} and (2) the total H I column density N_{HI} . Although the H I Lyman series lines are sensitive to the component structure and the Doppler parameters (also known as b -values) of the ‘clouds’ comprising an LLS, the opacity blueward of λ_{912} is insensitive to these details. Furthermore, the SDSS spectra are generally of too poor quality to constrain such structure using the observed Lyman series lines. Therefore, our model of an LLS assumes a single cloud with a Doppler parameter of $b = 30 \text{ km s}^{-1}$. An implication of this pa-

⁶ <http://www.ucolick.org/~xavier/IDL>

⁷ This stack is not optimal for deriving Ly α forest statistics (Dall’Aglio et al. 2008).

parameterization is that two systems with small redshift separation are modeled as a single system with the total of the N_{HI} values. Our tests with mock spectra (§ 7) indicate that two absorbers with $\delta z < 0.1$ are often indistinguishable from a single LLS. The survey presented here, therefore, refers to LL absorption smoothed over a redshift interval of $\delta z \approx 0.1$. We return to this point in our presentation and discussion of the survey results.

We have developed an algorithm (*sdss_findlls*) to automatically search for and characterize LLS absorption in quasar spectra. In brief, the code generates a set of model spectra for the line and continuum opacity of a single LLS with redshifts covering $z = z_0 = (\lambda_0/\lambda_{912} - 1)$ to $(z_{\text{em}} + 0.2)$ where λ_0 is the starting wavelength of the SDSS spectrum and z_{em} is the quasar emission redshift reported in the DR7⁸. The grid of models assumes N_{HI} column densities $\log N_{\text{HI}} = 16.0, 16.2, 16.4, \dots, 19.8$ and a Doppler parameter $b = 30 \text{ km s}^{-1}$. We implement a grid with 0.2 dex spacing in N_{HI} because very few of the spectra have sufficient S/N to provide a more precise estimate. Furthermore, we estimate systematic uncertainties (e.g. related to continuum placement, sky subtraction) to be of this order. These models are convolved with the SDSS instrumental resolution and then applied to the absorbed quasar continuum. Finally, the code constructs a χ^2 grid in z_{LLS} and N_{HI} space, identifies the minimum χ^2 , and records the ‘best-fit’ values. This approach differs from previous methods which focused solely on the Lyman limit (e.g. Storrie-Lombardi et al. 1994) or relied on ‘by-eye’ analysis (Lanzetta 1991). In general, the spectra provide very little constraint on N_{HI} for values exceeding $10^{17.5} \text{ cm}^{-2}$ until the Ly α profile becomes damped (e.g. Prochaska et al. 2005). Therefore, we report lower limits to N_{HI} for any LLS with $\tau_{912} \geq 2$.

For sightlines with a single LLS having $N_{\text{HI}} > 10^{17.2} \text{ cm}^{-2}$ and good S/N_{912}^{A} (i.e. greater than 5 pix^{-1} at $\lambda_{912}^{\text{em}} \equiv \lambda_{912} \times [1 + z_{\text{em}}]$), we find that the automated algorithm is highly successful on its own. In practice, however, there are several aspects of the data and analysis that require visual inspection of the spectra and interactive modification to the model: First, many spectra have such low S/N that z_{LLS} and N_{HI} are poorly determined. In these cases, a local minimum in χ^2 can occur which gives a mis-estimate of these quantities. Second, the presence of multiple absorbers along the sightline (e.g. one or more pLLSs with a lower redshift LLS) gives a spectrum that cannot be well modeled by a single LLS. Third, a non-negligible number of the spectra retrieved from the SDSS database purported to be high z quasars are either at a lower redshift or are another class of astronomical object altogether. Fourth, we found that half of the absorbed continuum models required scaling to higher or lower value by greater than 10%. Finally, we prefer to avoid quasars with with strong broad absorption line (BAL) or associated systems to focus the analysis on intervening LLSs.

Given the above complications to an automated analysis, we built a graphical user interface (GUI) within the IDL software package (*sdss_chklls*; bundled within XIDL) that inputs the data and best-fit LLS model for each object. Two of the authors (JXP and JMO)

⁸ Modified by the analysis of Prochaska et al. (2008) where applicable for quasars from the DR5 release.

TABLE 2
SDSS-DR7 INTERVENING $\tau_{912} \geq 2$ LLS SURVEY

Quasar	z_{em}	$z_{\text{start}}^{S/N=2}$	$z_{\text{start}}^{S/N=3}$	z_{LLS}
$z_{\text{em}} < 3.6$				
J001328.21+135828.0	3.575	3.443
J015741.56–010629.6	3.564	3.387	3.387	3.387
J073947.17+445236.7	3.575	3.300
J074914.13+305605.8	3.436	3.300	3.300	...
J075303.34+423130.7	3.590	3.300	3.300	...
J075859.81+165811.8	3.439	3.366	...	3.366
J080025.10+441723.1	3.554	3.300	3.362	...
J080525.53+123438.7	3.425	3.300	3.300	...
$z_{\text{em}} \geq 3.6$				
J001115.23+144601.8	4.967	4.567
J001820.71+141851.5	3.936	3.536	3.596	...
J004219.74–102009.4	3.880	3.633	3.633	3.633
J010619.24+004823.3	4.449	4.049	4.049	...
J011351.96–093551.0	3.668	3.615	3.615	3.615
J012403.77+004432.7	3.834	3.434	3.434	...
J015048.82+004126.2	3.702	3.302	3.302	...
J015339.61–001104.8	4.194	3.879	...	3.879

NOTE. — [The complete version of this table is in the electronic edition of the Journal. The printed edition contains only a sample.]

used this GUI to validate and/or modify all of the models. These authors flagged erroneous spectra (159 examples), strong BAL or associated absorption (quasars showing very strong C IV, N V, and O VI absorption; 290 quasars), or data with such low S/N that any analysis was deemed impossible (114 spectra). For the remainder of sightlines, the authors could modify the continuum (via a multiplicative scalar; Table 1) and/or change the model of LLS absorption (i.e. z_{LLS} , N_{HI}). This includes absorption due to candidate pLLSs. In many cases, z_{LLS} was modified to correspond to the strongest, local Ly α absorption line at $\lambda = (1 + z_{\text{LLS}}) \times 1215.67 \text{ \AA}$, especially for those systems that also showed absorption at the expected wavelength for Ly β .

After every sightline was analyzed in this manner, the results from the two authors were compared to assess consistency. Roughly half of the spectra were reviewed because of conflicts in the models. The majority of these were associated with the absorbed continuum placement (typically offsets of 5–10%) which implied differences in the search path of $|\Delta z| > 0.1$ (see § 6). In the majority of these cases, we simply averaged the two estimations of the continuum. The second most frequent conflict was on the definition of strong BAL absorption, primarily because we did not adopt uniform or strict criteria. In most cases, we conservatively excluded the sightline. There were also ≈ 100 cases where one author estimated $\log N_{\text{HI}} = 17.4$ when the other estimated $\log N_{\text{HI}} = 17.6$, i.e., straddling the $\tau_{912} = 2$ boundary that defines our LLS search. These were especially scrutinized for the presence of higher-order Lyman series lines. Where necessary, the final best-estimate for N_{HI} was deferred to the third author (GW).

Tables 2 and 3 list the set of Lyman limit systems identified in the SDSS-DR7 for systems that (respectively) influence our statistical analysis and otherwise. For each system, we list our best estimate for z_{LLS} and the N_{HI}

TABLE 3
SDSS-DR7 NON-STATISTICAL LLS SYSTEMS AND CANDIDATES

Quasar	z_{em}	z_{LLS}	$\log N_{HI}^a$	S/N^b
J000238.41–101149.8	3.938	3.809	17.2	0.7
J000300.34+160027.7	3.698	3.570	17.2	1.3
J000303.34–105150.6	3.646	3.467	17.6	1.5
J000335.21+144743.6	3.484	3.498	16.6	0.9
J000536.38+135949.4	3.686	3.580	19.0	1.1
J000730.82+160732.5	3.501	3.511	19.8	1.3
J001115.23+144601.8	4.967	3.995	17.8	2.6
J001134.52+155137.3	4.325	4.348	19.8	1.1
J001328.21+135828.0	3.575	3.282	19.8	1.7
J001747.90+141015.7	3.955	3.925	17.4	1.0
J001813.88+142455.6	4.235	4.151	17.2	1.6
J001820.71+141851.5	3.936	3.456	17.2	2.4
J001918.43+150611.3	4.134	4.053	17.8	1.2
J001950.05–004040.7	4.327	4.047	18.4	1.8
J002120.05+155125.7	3.698	3.671	17.8	2.0
J002614.69+143105.2	3.973	3.895	19.8	1.3

NOTE. — [The complete version of this table is in the electronic edition of the Journal. The printed edition contains only a sample.]

^aThe N_{HI} values listed serve as a rough estimate. Typical uncertainties for systems with $N_{HI} < 10^{17.5} \text{ cm}^{-2}$ are at least 0.2 dex.

^bEstimate of the S/N of the absorbed continuum (ignoring the effects of pLLS) at $\lambda = \lambda_{912}(1 + z_{LLS})$.

value. Because the data offer minimal constraint on N_{HI} for values exceeding $10^{17.5} \text{ cm}^{-2}$, in the statistical sample we only report a lower limit to N_{HI} for all systems with best-estimates of $N_{HI} \geq 10^{17.5} \text{ cm}^{-2}$. For the pLLSs, the typical 1σ uncertainty is approximately 0.2 dex for $N_{HI} \geq 10^{17} \text{ cm}^{-2}$ and is dominated by systematic error in the continuum placement and the stochastic nature of IGM opacity. As noted above, z_{LLS} was frequently modified in the interactive analysis to correspond to strong Ly α and Ly β lines. Our analysis of mock spectra indicate typical redshift uncertainties of $\sigma(z) < 0.02$ with occasional ‘catastrophic failures’ due to line-blending or spurious spectra (§ 7). No attempt was made to improve this estimate by searching for the presence of metal-line absorption (e.g. C IV) outside the Ly α forest. There is a tendency, both in the automated algorithm and in interactive analysis, to set z_{LLS} at the highest value possible that can be accommodated by the data. To this extent, we suspect that there is a modest bias in our z_{LLS} values to slightly higher redshifts (less than 0.01 on average, but with the occasional large offset).

Figure 3 shows a representative sample of four quasar spectra, zoomed into the region blueward of Ly β , with the absorbed continuum and LLS models indicated. We provide snapshots of the LL region for all quasar spectra in the statistical sample online⁹.

6. SURVEY PATH

Analogous to galaxy surveys where one defines a search volume based on the depth of imaging and spectroscopic follow-up, measurements of the incidence of quasar absorption line systems requires an estimate of the total spectral path sensitive to a robust search. This is generally referred to as the redshift path covered (by translating observed wavelength into redshift). For the survey

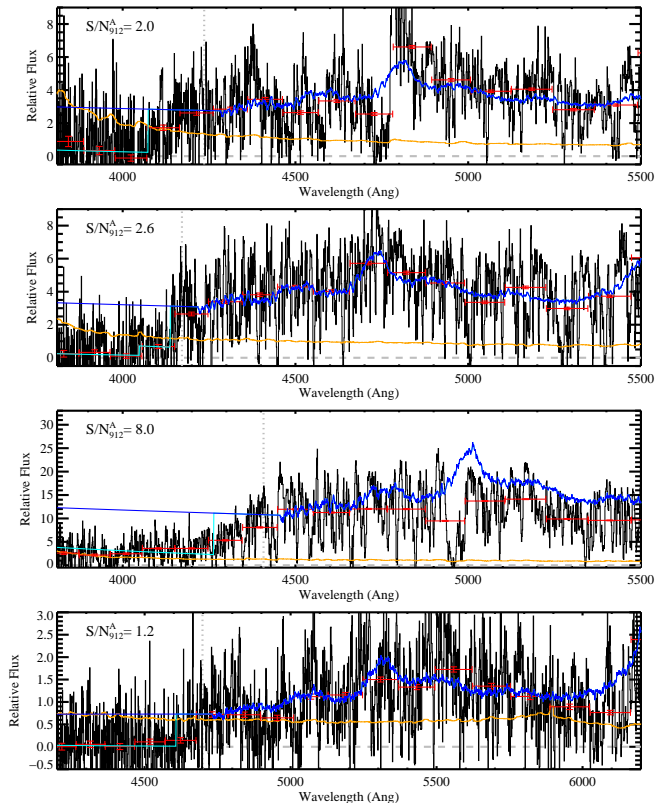


FIG. 3. — Representative SDSS-DR7 spectra of quasars from our statistical survey. Each example shows the absorbed continuum model (dark blue) and the model that includes LL absorption (cyan). The smoothed 1σ error array is given by the orange curve. For this presentation, we have not shown the Lyman series in the model. The vertical dotted line indicates the Lyman limit wavelength in the quasar rest-frame, i.e. at $\lambda_{912}^{em} = \lambda_{912}(1 + z_{em})$. The red bins indicate the mean flux in intervals of 100 pixels. The top panel shows a typical example of a $\tau_{912} \geq 2$ LLS in data that just satisfies our S/N_{912}^A criterion. The next lower panel shows an example where we identify a pLLS candidate and then a $\tau_{912} \geq 2$ LLS. The next lower panel shows a high S/N_{912}^A example whose quasar spectrum rapidly declines with decreasing wavelength below λ_{912}^{em} . This absorbed continuum was modelled by including a pLLS candidate. The lowest panel shows a low S/N_{912}^A example where a $\tau_{912} \geq 2$ LLS is apparent.

of LLSs, we have adopted the following criteria for including spectral regions in the search. These are based on our automated and interactive analysis of the SDSS spectra, our modeling of Keck/LRIS follow-up spectra, and our analysis of simulated spectra (§ 7, Appendix A):

1. The search path will begin at a minimum redshift of $z_{start} \geq 3.3$
2. For the intervening LLS sample, the search path ends at the redshift z_{end} corresponding to 3000 km s^{-1} (relativistic) blueward of the quasar redshift z_{em} .
3. The absorbed continuum flux must exceed twice the estimated error array, i.e. S/N_{912}^A .
4. The search path begins at a maximum offset of $\delta z = z_{em} - z_{start} \leq 0.4$.

The first criterion is motivated by the starting wavelength of the SDSS spectra ($\lambda_0 \approx 3800\text{\AA}$) and the poorer quality of the data at the bluest wavelengths. For redshifts less than 3.3, there is insufficient spectral coverage

⁹ <http://www.ucolick.org/~xavier/SDSSLLS>

and/or data quality to confidently assess the presence of an LLS. The second criterion minimizes the influence of the quasar and its environment on the analysis. This criterion is relaxed in the study of PLLSs.

The third criterion is the most subjective, yet important, for setting the redshift survey path of each quasar. Algorithmically, we impose this constraint by identifying the first pixel blueward of $\lambda_{912}^{\text{em}} \equiv \lambda_{912}(1 + z_{\text{em}})$ where our model of the absorbed quasar continuum falls below twice the median-smoothed (15 pixels) 1σ error array.

This pixel defines the starting redshift $z_{\text{start}}^{S/N^A=2}$ corresponding to a $S/N_{912}^A=2$ limit. If the first pixel blueward of $\lambda_{912}^{\text{em}}$ does not satisfy the S/N threshold, the quasar has zero redshift path, i.e. $z_{\text{start}} = z_{\text{end}}$. One can, of course, define starting redshifts corresponding to higher (or lower) S/N_{912}^A limits; indeed, our fiducial choice of $S/N_{912}^A=2$ should be considered arbitrary, although it is guided by our analysis of real and simulated spectra. And to avoid a systematic bias associated with pLLSs (see § 7.3), one must choose the S/N_{912}^A criterion to be sufficiently high to discover $\tau_{912} \geq 2$ LLS even in the presence of a pLLS¹⁰. We investigate the impact of this choice on our results later in the manuscript. Finally, our fourth criterion is imposed to mitigate the cumulative effects that pLLSs can have on our ability to detect LLS with $\tau_{912} \geq 2$. That is, trials with mock spectra (§ 7) indicate that multiple pLLSs along a single sightline may prevent the detection of a $\tau_{912} \geq 2$ LLS and that this bias is minimized provided $\delta z < 0.4$. Furthermore, we find that the extrapolation of the absorbed continuum from the quasar’s Lyman limit often is a poor model for $\delta z > 0.4$.

The starting redshift is further modified by the presence of Lyman limit absorption. In the case of a $\tau_{912} \geq 2$ absorber, the quasar flux is severely depressed below $\lambda = \lambda_{912}(1 + z_{\text{LLS}})$ and we terminate the search path at this wavelength. Specifically, this implies $z_{\text{start}} \geq z_{\text{LLS}}$ for all sightlines with an $\tau_{912} \geq 2$ LLS. For sightlines where one or more pLLSs are identified¹¹, we had originally intended to terminate the search once the absorbed quasar continuum convolved with the pLLS absorption failed to satisfy the S/N threshold. In our analysis of mock spectra, however, we found that this introduces a “pLLS-bias” where the incidence of $\tau_{912} \geq 2$ LLS is overestimated (§ 7.3). In part, our $S/N_{912}^A=2$ threshold is chosen so that one can robustly search for $\tau_{912} \geq 2$ LLSs even along sightlines where one or more pLLSs are present.

Table 2 presents the list of quasars in SDSS-DR7 that (i) have $3.6 \leq z_{\text{em}} \leq 5$, (ii) were not identified to exhibit strong BAL signatures, and (iii) have $3.3 \leq z_{\text{start}}^{S/N^A=2} < z_{\text{em}}$. There are 469 quasars satisfying these criteria. For each sightline, we list the starting redshifts for $S/N_{912}^A=2$ and 3 limits. We report results for these two values of the S/N threshold to search for data-quality biases. Table 2 also lists all Lyman limit systems with $z_{\text{LLS}} \geq z_{\text{start}}^{S/N^A=2}$.

¹⁰ Contrary to some of the earliest work on LLSs (e.g. Tytler 1982), we do not use survival statistics to estimate the number of LLSs at redshifts below any observed LLS.

¹¹ Again, all pLLSs should be considered candidates. Some of the spectral features modeled as pLLSs are instead due to unusual variations in the absorbed quasar continuum (e.g. highly reddened quasars).

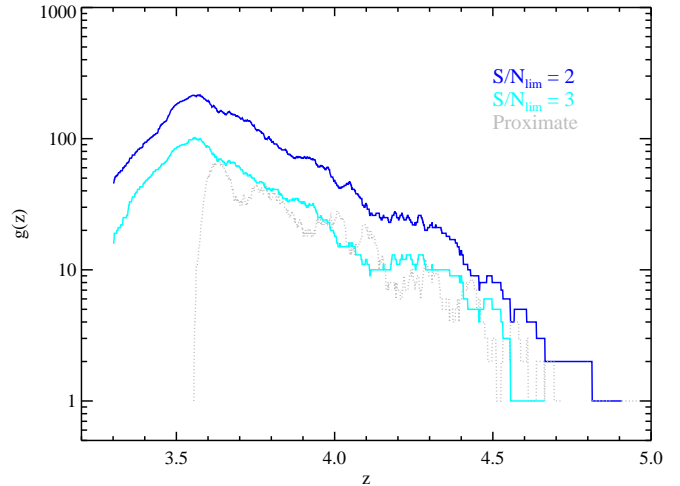


FIG. 4.— Summary of the redshift path surveyed in the SDSS-DR7 for $\tau_{912} \geq 2$ LLS absorption assuming S/N_{912}^A thresholds of 2 and 3 (solid curves). Specifically, $g(z)$ represents the number of unique quasars in the SDSS that provide a search for LLSs over the interval $dz = 0.001$ at redshift z . The dotted curve, meanwhile, represents the same quantity but for proximate LLSs (PLLSs; systems within $\delta v = 3000 \text{ km s}^{-1}$ of the quasar) and corresponds to a $S/N_{912}^A=2$ threshold. These curves fall rapidly for $z < 3.6$ because we limit the analysis to quasars with $z_{\text{em}} \geq 3.6$. The non-monotonic nature of $g(z)$ is due primarily to the presence of LLSs along the quasar sightlines which stochastically truncate the search path.

We do list these quantities for quasars with $z_{\text{em}} < 3.6$, but these were not included in our final statistical analysis because of the bias related to SDSS targeting criteria previously mentioned by PWO09.

Using the values presented in Table 2, it is straightforward to calculate z_{end} and the redshift search path for each quasar: $\Delta z_i = z_{\text{end}} - z_{\text{start}}$. For a given S/N_{912}^A limit, the total search path for the full dataset is

$$\Delta z_{\text{TOT}} = \sum \Delta z_i \quad (8)$$

We calculate $\Delta z_{\text{TOT}}^{S/N=2} = 96$. To maintain a homogeneous sample and set of search criteria, we do not include previous studies in our analysis. We compare against previous results in § 9.

In Figure 4, we present the sensitivity function $g(z)$ which expresses the number of SDSS quasars at redshift z where a robust search for LLSs is possible. The several solid curves represent differing S/N_{912}^A limits for the survey. We also present the sensitivity function for proximate LLSs (PLLSs) which corresponds to the sample of quasar spectra that satisfy the $S/N_{912}^A \geq 2$ criterion at 3000 km s^{-1} blueward of z_{em} .

With the definition of the search path and the identification of the Lyman limit systems along each sightline (§ 5), it is straightforward to calculate the incidence of intervening $\tau_{912} \geq 2$ LLS per redshift interval, $\ell_{\tau \geq 2}(z)$. The standard estimator is to compare the total number of LLSs against the total survey path in discrete redshift intervals. We will return to evaluate $\ell_{\tau \geq 2}(z)$ and discuss the values after exploring several sources of systematic error.

With a survey the size of SDSS, one can quickly reduce the statistical noise in measurements to very small levels. In this regime, one must carefully assess all sources of systematic error as these may dominate the measurement uncertainty. To this end, we have conducted a range of tests with mock spectra as described in this section. The casual reader may wish to skip to the summary of this section (§ 7.6)

7.1. Mock Spectra Construction

We generated a set of 800 mock SDSS quasar spectra and analyzed them in the same way as the real data in order to assess bias and completeness in our LLS survey. The H I forest absorption spectra were generated via a Monte Carlo routine similar to the one described in Dall’Aglio et al. (2008), assuming that the Ly α forest is well characterized by three independent distributions: (i) the Ly α line-incidence $\ell_\alpha(z) \propto (1+z)^\gamma$, (ii) the H I column density distribution $f(N_{\text{HI}}) \propto N_{\text{HI}}^\beta$, and (iii) the Doppler parameter distribution parameterized as $f(b) \propto b^{-5} \exp[-b_\sigma^4/b^4]$ (Hui & Rutledge 1999). Each simulated line of sight was filled with H I Ly α absorption lines at $2 < z < 4.6$ until the H I Ly α effective optical depth was consistent with Faucher-Giguère et al. (2008b), both in normalization and redshift evolution. We did not model the $z \sim 3.2$ dip in the effective optical depth measured by Faucher-Giguère et al., and instead adopted a simple power-law $\tau_{\text{eff}}^\alpha = 0.0011(1+z)^{4.23}$. If the number of lines in a given patch of the forest is Poisson-distributed, a power-law line density evolution $\ell_\alpha(z) \propto (1+z)^\gamma$ yields a power-law effective optical depth evolution $\tau_{\text{eff}}^\alpha \propto (1+z)^{\gamma+1}$ (Zuo 1993). The column density distribution was modeled with a single power-law index $\beta = -1.5$ for $12 < \log(N_{\text{HI}}) < 19$, but with a 0.5 dex break at $\log(N_{\text{HI}}) = 14.5$ in order to account for the dearth of high column density lines, consistent with observations (e.g. Hu et al. 1995; Kim et al. 2002, and our own inferences, § 8.3). For the Doppler parameter distribution we set $b_\sigma = 24 \text{ km s}^{-1}$ (Kim et al. 2001).

Because SLLSs ($19 \leq \log(N_{\text{HI}}) < 20.3$) and DLAs ($\log(N_{\text{HI}}) \geq 20.3$) have different column density distributions and are usually excluded in measurements of τ_{eff}^α , these were added after the $\log(N_{\text{HI}}) < 19$ line forest converged to the chosen $\tau_{\text{eff}}^\alpha(z)$. To constrain the redshift evolution of SLLSs, we combined the sample by O’Meara et al. (2007) and the lower limit given in Rao et al. (2006), yielding $\ell_{\text{SLLS}}(z) \sim 0.066(1+z)^{1.70}$. For the SLLS column density distribution we adopted $\beta = -1.4$ (O’Meara et al. 2007). The DLAs were modeled via $\ell_{\text{DLA}}(z) = 0.044(1+z)^{1.27}$ (Rao et al. 2006) and $\beta = -2$ (Prochaska et al. 2005), ignoring deviations in $f(N_{\text{HI}}, X)$ from a single power law. The Doppler parameter distribution was left unchanged.

With the overall opacity of the modeled Ly α forest consistent with observations, and the high column density systems incorporated, we used the generated line lists to compute H I Lyman series (up to Ly30) and Lyman continuum absorption spectra. In total we computed 800 different lines of sight for quasars in the redshift range of our sample, 160 each at $z = 3.4, z = 3.6, z = 3.8, z = 4.0$ and $z = 4.2$, respectively. From these we then generated mock SDSS spectra. First, the resolved H I forest spectra were multiplied onto synthetic quasar SEDs generated from principal component spectra (Suzuki 2006).

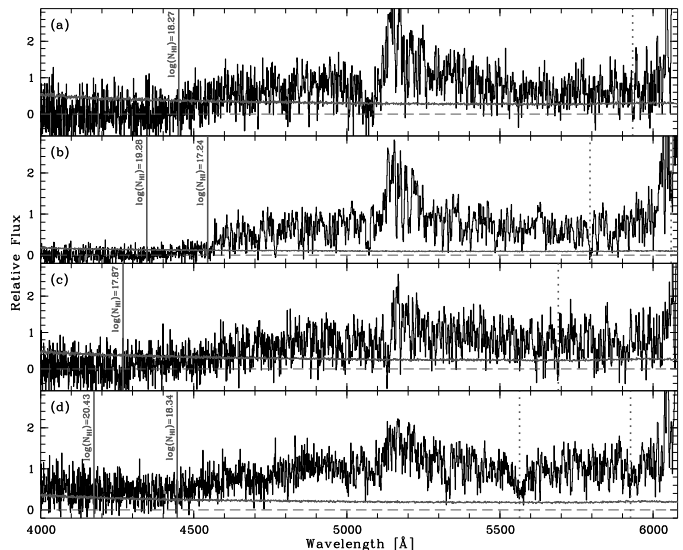


FIG. 5.— This figure presents a sample of the mock spectra analyzed in the paper. (a): A spectrum representative of the typical data quality ($S/N_{912}^A \sim 2$ at the Lyman limit of the quasar). There is a LLS ($z = 3.88059, \log N_{\text{HI}} = 18.27$) that can be easily identified at this S/N_{912}^A . Two systems at higher z with $N_{\text{HI}} \approx 10^{16} \text{ cm}^{-2}$ modify the continuum but do not produce a $\tau_{912} \geq 2$ LLS; (b): A high-S/N spectrum ($S/N_{912}^A \sim 6$ at the Lyman limit of the quasar), rendering its partial LLS ($z = 3.98387, \log N_{\text{HI}} = 17.24$) easily visible. An additional SLLS at lower redshift ($z = 3.76609, \log N_{\text{HI}} = 19.28$) sets the flux to zero at the Lyman limit. (c): This mock spectrum shows a slow ‘roll-off’ in flux blueward of the quasar’s Lyman limit. There is a LLS ($z = 3.68084, \log N_{\text{HI}} = 17.87$), and five systems with $16 < \log N_{\text{HI}} < 17$ at higher z that produce the roll-off. The S/N at the Lyman limit of the quasar is quite low ($S/N \sim 1.5$) and the intervening systems further decrease the S/N, rendering the LLS invisible. (d): A spectrum with strongly under-subtracted sky background. The first strong system encountered is a LLS ($z = 3.87495, \log N_{\text{HI}} = 18.34$), but the flux is above zero even after hitting a DLA ($z = 3.57678, \log N_{\text{HI}} = 20.43$). One can assess that the sky subtraction is poor, because the Ly α profile of the DLA does not saturate. The solid/dotted vertical lines in each panel trace the Lyman limit/Ly α line of each absorber.

We then degraded the resolution of the mock spectra to $R = 2000$ by convolving them with a Gaussian, and rebinned them to $\delta v = 69 \text{ km s}^{-1}$, matching the approximate resolution and pixel size of the SDSS spectra. Finally, we added Gaussian noise to the mock SDSS spectra. In each mock spectrum, the S/N was normalized in the quasar continuum at 1450 \AA and varied as a function of flux and wavelength according to the throughput of the SDSS spectrograph. The sky level was approximated as a constant and readout noise was also incorporated. Finally, for a subset of the mocks we imposed a sky subtraction error implemented by subtracting/adding a constant to the spectrum. These were generated to mimic such systematic errors that occasionally occur in the SDSS spectra.

Four representative examples are shown in Figure 5.

7.2. LLS Recovery and Sky Subtraction Bias

Two of the authors (JXP, JMO) analyzed mock spectra using the identical tools and procedures applied to the SDSS spectra; these steps were done without knowledge of the mock line distribution and column densities (constructed by author GW). The integrated results for the two authors were nearly identical; the following discussion and figures refer to the results related to JXP.

Figure 6 summarizes the completeness and several bi-

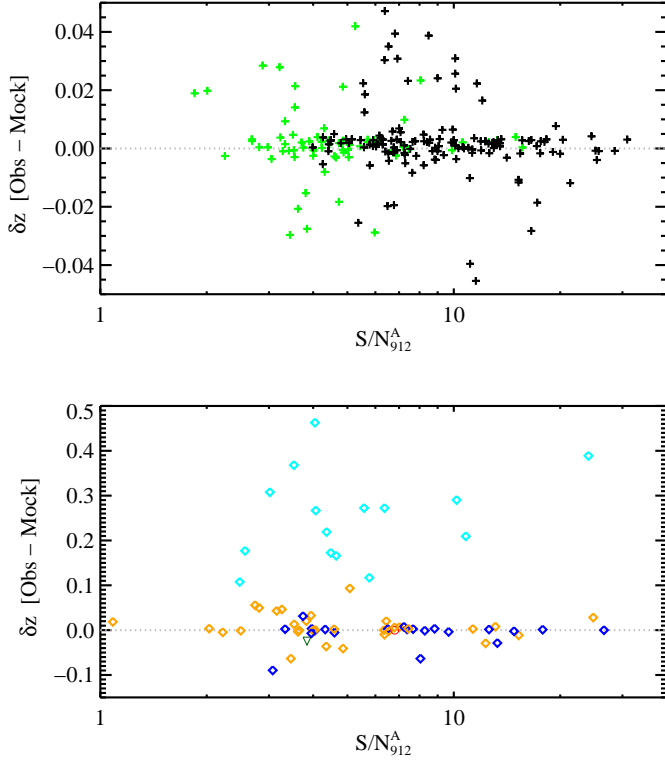


FIG. 6.— Offset in redshift δz for the ‘observed’ LLS and pLLS from the z_{abs} value of the nearest ‘true’ $\tau_{912} \geq 2$ LLS in our mock spectra. The analysis is restricted to the highest z_{abs} LLS along each sightline. In the upper panel, we show the δz value for sightlines where a LLS was ‘observed’ and actually exists. Lighter/darker (green/black) points correspond to LLSs discovered outside/within the statistical survey path (i.e. $S/N_{912}^A=2$). These are the majority of cases ($> 80\%$) and we find small δz values with a small, but important bias to $\delta z > 0.01$. In the lower panel, we show false negatives (diamonds) and false positive (triangles) detections. The former correspond to a true LLS that was observed as ($\delta z < 0.1$) or hidden by a pLLS ($\delta z > 0.1$). The misidentifications ($\delta z < 0.1$) are dominated by the mock spectra with large underestimates in the sky background. The dominant effect of a sky subtraction bias is an underestimate in the incidence of LLSs. For the misidentifications with $\delta z < 0.1$, the dark points indicate systems that satisfy all of the survey criteria (e.g. $z > 3.3$, $S/N_{912}^A \geq 2$).

ases uncovered by our analysis. In the top panel, all cases where a mock $\tau_{912} \geq 2$ LLS exists with $z_{\text{abs}} > 3.2$ and an LLS was ‘observed’ are presented; these correspond to $> 80\%$ of the cases. Specifically, we plot the offset δz between the true and observed LLS absorption redshifts as a function of the S/N_{912}^A of the spectrum. We find excellent agreement (small δz), nearly independent of the S/N_{912}^A of the data. There are, however, a number of cases with $\delta z > 0.01$, primarily related to the blending of absorption lines (see below).

The lower panel in Figure 6 presents those cases that are false negatives (diamonds) and false positives (triangles). The latter are very rare. The former, however, did occur quite often in our analysis and can be divided into two classes: (i) cases with $|\delta z| < 0.05$ which are proper false negatives, i.e. true $\tau_{912} \geq 2$ LLS that were modeled as a pLLS; (ii) cases with $\delta z > 0.1$ which are sightlines where a higher z pLLS precluded the detection of a lower z LLS. The majority of the latter cases are due to bona-fide pLLS at higher z which greatly diminish the S/N

of the spectra at shorter wavelengths and ‘obscure’ the presence of a $\tau_{912} \geq 2$ LLS. Almost none of these cases, however, satisfy the selection criteria established in § 6; either the data have too low S/N_{912}^A or the absorption redshift of the LLS gives $z_{\text{em}} - z_{\text{abs}} \geq 0.4$.

The first class of false negatives, meanwhile, are almost exclusively associated with spectra that had systematically low estimates for the sky background. In these cases, a $\tau_{912} \geq 2$ LLS has an apparent flux at $\lambda < \lambda_{912}$ and therefore was modeled as a pLLS. This is the dominant effect of a sky subtraction bias. Although our mock spectra had even numbers of over and under-subtracted sky backgrounds, only the former are relatively easy to identify (large regions of spectra are significantly negative) and ignore. The net effect of a random sky subtraction error is a systematic underestimate in the incidence of LLS. We stress, however, that the magnitude and frequency of poor sky subtraction in the mock spectra was intentionally elevated so that we could explore these effects. The incidence of such effects within the SDSS spectra is much lower, an assertion supported by our follow-up spectra with Keck/LRIS (Appendix A). Therefore, we are confident that the sky subtraction bias gives rise to a less than 10% systematic error for $\ell_{\tau \geq 2}(z)$.

7.3. The pLLS Bias

Originally, we intended to perform a search for LLSs in spectra with $S/N_{912}^A=1$ to maximize the pathlength of the survey (a nearly $4\times$ increase over $S/N_{912}^A=2$). Our tests with mock spectra and follow-up observations with Keck/LRIS (Appendix A) indicated that we could robustly identify $\tau_{912} \geq 2$ LLS in such data. We also noted, however, that many of the spectra showed pLLS candidates which reduced the S/N_{912}^A to below 1 and made the search for $\tau_{912} \geq 2$ LLS much more challenging. Our response was to redefine the search path by attenuating the absorbed continuum due to any identified pLLS candidates and then reapply the S/N_{912}^A criterion for the remaining $z < z_{\text{pLLS}}$ spectral range. With this approach, the search path was frequently terminated by the presence of a pLLS candidate.

In principle, this modification should provide an unbiased search for $\tau_{912} \geq 2$ LLS. Our trials with mock spectra, however, revealed an insidious bias associated with this redefinition of the search path. Specifically, it is very difficult to identify pLLSs when they occur at a small redshift offset ($\delta z \lesssim 0.1$) redward from a $\tau_{912} \geq 2$ LLS. In these cases, instead of the search being terminated at the redshift of the pLLS such that the lower z LLS is not included in the survey, it is the pLLS that is ignored and the LLS is included within the statistical sample. Furthermore, the redshift of the recovered LLS is biased to a higher value which reduces the survey pathlength by a small but non-negligible quantity. Together, these two effects lead to an overestimate of $\ell_{\tau \geq 2}(z)$ by values ranging from 30 – 50%. Furthermore, we find that it is very difficult to precisely estimate the magnitude of this systematic bias for it depends sensitively on $\ell_{\tau \geq 2}(z)$, the incidence of pLLS, and the quasar z_{em} distribution. In our opinion, one cannot robustly correct for this systematic pLLS bias and we caution against performing any analysis that would be subject to it. For these reasons, we *ignore* pLLS when defining the survey path based on a signal to noise criterion and performing the search for

$\tau_{912} \geq 2$ LLS. With this approach, one must have sufficient S/N_{912}^A to identify LLS even when one or more pLLS modify the absorbed continuum. This last point motivated our decision to restrict the survey to spectra with $S/N_{912}^A \geq 2$.

7.4. The Blending Bias

As noted in the previous sub-section, LLS and pLLS that lie close to one another in redshift are very difficult to distinguish as individual systems. This is even true in the limit where one has spectra with exquisite S/N and resolution when $\delta z < 0.1$ (or less in the case of high resolution echelle observations). With SDSS spectra, the limited information provided by the Lyman limit and the strongest Lyman series lines is insufficient to robustly distinguish multiple LLSs from a single system. This leads to a “blending bias” that manifests itself in several ways.

First, the blending bias increases the number of LLSs observed because pairs of pLLSs blend together to give a single system with $\tau_{912} \geq 2$. Second, the absorption redshifts of the LLSs are shifted to higher redshifts because one generally adopts z_{LLS} from the higher of the pair of systems. This leads to a smaller survey path and possibly a higher inferred incidence of LLSs. More importantly (see below), many LLSs are shifted into the proximate region of the quasar. This causes an underestimate of $\ell_{\tau \geq 2}(z)$ for intervening LLSs and an overestimate of pLLSs.

We explored the quantitative effects of the blending bias with the following analysis. We constructed a set of mock absorption lines for each quasar in the statistical survey (Table 2) with an incidence set to match our measurements (§ 8.1). Specifically, we adopted an N_{HI} frequency distribution

$$f(N_{\text{HI}}, z) = CN_{\text{HI}}^{\beta} \left(\frac{1+z}{1+z_*} \right)^{\gamma} \quad (9)$$

with $\beta = -1.3$ for $10^{16.5} \text{ cm}^{-2} \leq N_{\text{HI}} \leq 10^{19.5} \text{ cm}^{-2}$ and $\beta = -2$ for $N_{\text{HI}} \geq 10^{19.5}$, $z_* = 3.7$, $\gamma = 5.1$ and $C = 1.244 \times 10^5$. From the mock absorber list we identified all LLSs with $N_{\text{HI}} \geq 10^{17.5} \text{ cm}^{-2}$. This formed the control sample. Then, we blended together all systems with $|\delta z| \leq \delta z_j$ where $\delta z_j = [0.01, 0.05, 0.1, 0.2]$ and re-identified systems satisfying $N_{\text{HI}} \geq 10^{17.5} \text{ cm}^{-2}$. When blending two or more systems together, we set z_{abs} to the maximum of all the lines. Finally, we calculated the incidence of LLSs using the survey path and LLSs for each δz_j .

Figure 7a presents the results of the blending bias in terms of the enhancement/decrement of the incidence of $\tau_{912} \geq 2$ LLS relative to the perfect model ($\delta z_j = 0$). For $\delta z_j < 0.1$, there is only a small and ignoreable effect. For $\delta z_j \geq 0.1$, however, we predict a systematic underestimate for the incidence of intervening LLSs, especially at $z > 4$ where the absolute incidence is highest. This deficit in $\ell_{\tau \geq 2}(z)$ runs contrary to expectation and is entirely due to the redshift bias where the blended LLSs end up with z_{LLS} within the proximate region. In turn, we predict a systematic over-estimate of $\ell_{\tau \geq 2}(z)$ for PLLSs (Figure 7b).

Our experiments with mock spectra indicate that we commonly blend together systems with $\delta z_j = 0.05$ to 0.1,

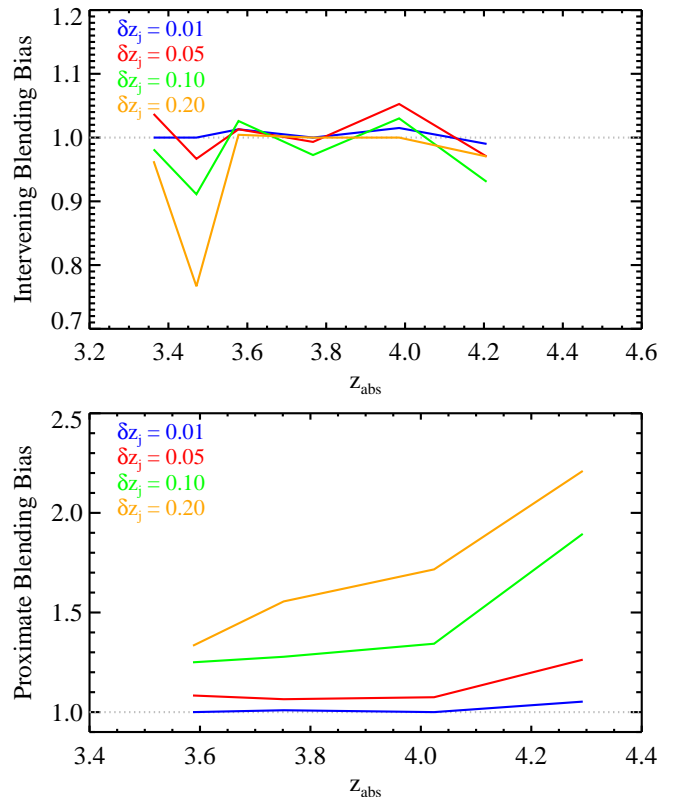


FIG. 7.— Blending bias (enhancement/decrement of $\ell_{\tau \geq 2}(z)$ relative to no bias) for mock absorption line systems for (upper) intervening $\tau_{912} \geq 2$ LLSs and (lower) proximate $\tau_{912} \geq 2$ LLSs. The absorption line statistics were set to roughly match the observed incidence. Even for blending with redshifts $\delta z_j = 0.2$, the bias for intervening systems is relatively small. In contrast, the blending bias systematically elevates $\ell_{\tau \geq 2}(z)$ for PLLSs, especially at $z > 4$.

with a weak dependence on redshift or S/N. We conclude, therefore, that the effects of the blending bias on our SDSS analysis are $< 10\%$ for measurements of $\ell_{\tau \geq 2}(z)$ for intervening LLSs. This is below the current level of the statistical error and we will ignore it in the presentation of the results and discussion. For the PLLSs, the effect for $\delta z_j = 0.1$ ranges from 20 – 90% and we will report our results on $\ell_{\tau \geq 2}(z)$ for these absorbers as upper limits, especially for $z_{\text{abs}} > 4$.

Before closing this section, we stress that the blending bias affects all previous and future LLS surveys. In particular, we caution that the incidence of LLSs cannot trivially be used to constrain the H I frequency distribution $f(N_{\text{HI}}, X)$, because the latter assumes that every absorption system is a unique, identifiable line. For the LLSs in particular (but this is also true for the Ly α forest), blending smears these lines over non-negligible redshift intervals ($\delta z \approx 0.1$) and this affect must be considered when comparing against theoretical line densities.

7.5. Continuum Uncertainty

An important systematic uncertainty in our analysis is the placement of the absorbed quasar continuum. As described in § 4, the continuum for each quasar spectrum was determined from an automated fit of a template model to the data. Each continuum was then reviewed by two authors (JXP, JMO) and frequently scaled up/down by 5–10%. For our LLS survey, modifications to the con-

TABLE 4
LLS STATISTICS

z	ΔX	Δz^a	m_{LLS}^c	\bar{z}^a	$\ell_{\tau \geq 2}(z)^d$ ($S/N_{912}^A=2$)	$\ell_{\tau \geq 2}(z)^d$ ($S/N_{912}^A=3$)	$\ell_{\tau \geq 2}(X)^d$ ($S/N_{912}^A=2$)	Δr_{LLS}^e (Mpc)
Full Sample								
[3.30,4.40]	366.5	93.8	192	3.68	$2.05^{+0.15}_{-0.16}$	$2.11^{+0.22}_{-0.25}$	$0.52^{+0.04}_{-0.04}$	78
Redshift Intervals								
[3.30,3.40]	25.7	6.8	9	3.35	$1.31^{+0.43}_{-0.60}$	$2.28^{+0.84}_{-1.23}$	$0.35^{+0.11}_{-0.16}$	147
[3.40,3.50]	49.2	12.9	28	3.47	$2.17^{+0.40}_{-0.49}$	$2.03^{+0.55}_{-0.73}$	$0.57^{+0.11}_{-0.13}$	83
[3.50,3.65]	111.7	29.0	46	3.58	$1.59^{+0.23}_{-0.27}$	$1.44^{+0.33}_{-0.41}$	$0.41^{+0.06}_{-0.07}$	107
[3.65,3.90]	109.7	27.9	57	3.74	$2.05^{+0.27}_{-0.31}$	$2.37^{+0.44}_{-0.54}$	$0.52^{+0.07}_{-0.08}$	76
[3.90,4.10]	41.9	10.4	30	3.97	$2.89^{+0.52}_{-0.63}$	$2.45^{+0.76}_{-1.04}$	$0.72^{+0.13}_{-0.16}$	48
[4.10,4.40]	28.3	6.8	22	4.23	$3.22^{+0.68}_{-0.84}$	$3.44^{+1.02}_{-1.38}$	$0.78^{+0.16}_{-0.20}$	38

NOTE. — Unless specified otherwise, all quantities refer to the $S/N_{912}^A=2$ threshold. The cosmology assumed has $\Omega_\Lambda = 0.7$, $\Omega_m = 0.3$, and $H_0 = 72 \text{ km s}^{-1} \text{ Mpc}^{-1}$.

^aTotal redshift survey path for the $S/N_{912}^A=2$ criterion.

^bNumber of $\tau_{912} \geq 2$ LLS discovered in the survey path.

^cMedian absorption redshift of the LLS for the $S/N_{912}^A=2$ threshold.

^dLine densities of LLS with $\tau \geq 2$ per redshift dz or absorption length dX . Often written as dn/dz (or dN/dX) in the literature.

^eAverage proper distance between LLS with $\tau \geq 2$.

tinuum primarily modify the survey path; the estimates of τ_{912} are only affected if $\tau_{912} \lesssim 2$.

To test the sensitivity of our results to continuum placement, we reanalyzed the data after scaling each continuum up/down by 5 and 10%. We also considered a scenario where the scaling was random between $\pm 10\%$. We find that the estimates on the incidence of LLSs varies by 5 – 10% as the continua are modified. The effect, while due to systematic changes in the continuum, is not systematic. That is, a systematic increase in the continuum does not systematically increase/decrease the incidence of LLSs at all redshifts. Therefore, we conclude that continuum placement errors yield a random, non-negligible ($\approx 5 - 10\%$) uncertainty in the final results.

7.6. Summary

We have conducted an assessment of the systematic uncertainty related to surveying LLSs using mock spectra with idealized Ly α forest absorption yet realistic spectral characteristics (noise, resolution). Our analysis revealed an insidious bias associated with pLLSs that is best minimized by restricting the analysis to data with $S/N_{912}^A \geq 2$. We identified an unavoidable bias related to the blending of LLS and pLLS that implies a $\approx 10\%$ uncertainty in the measured incidence of LLSs. This bias becomes even more significant at $z > 4$ when the incidence of LLSs exceeds 3 per unit Δz . Finally, we found that continuum placement errors yield a random, non-negligible ($\approx 5 - 10\%$) uncertainty. Although higher S/N and spectral resolution will reduce some of these effects, we conclude that it will be difficult to avoid a systematic error of 10 – 20% using the standard approaches to surveying LLSs. We believe that future programs will require new techniques if higher precision measurements are desirable.

8. RESULTS

In this section, we present the principal results of our survey. We defer extended discussion of previous work and the implications of our analysis to the following section. Systematic biases and uncertainties in these results were discussed in the previous section and are summarized in § 7.6.

8.1. $\ell_{\tau \geq 2}(z)$: The Incidence of Intervening $\tau_{912} \geq 2$ LLSs per Redshift Interval

An LLS survey, by its nature, provides only a single observable quantity: the incidence of LLSs per redshift interval $\ell_{\tau \geq 2}(z)$. This quantity is independent of any assumed cosmology and consequently has limited physical meaning. Nevertheless, it is the proper starting point for describing our results.

Following standard practice, we estimate $\ell_{\tau \geq 2}(z)$ from the ratio of (N_{LLS}) the number of LLSs detected in a redshift interval to (Δz_{TOT}) the total search path for that redshift interval:

$$\ell_{\tau \geq 2}(z) = \frac{N_{\text{LLS}}}{\Delta z_{\text{TOT}}} \quad (10)$$

The statistical error in $\ell_{\tau \geq 2}(z)$ from this estimator is assumed to be dominated by the Poisson uncertainty in N_{LLS} . We have discussed a range of possible systematic uncertainties with this estimator in the previous section. Figure 8 presents the values of $\ell_{\tau \geq 2}(z)$ for the $S/N_{912}^A=2$ criterion in a set of arbitrary redshift intervals chosen to give $m_{\text{LLS}} \gtrsim 30$ systems per bin. Table 4 lists these values for S/N_{912}^A thresholds of 2 and 3; there is no obvious dependence with this threshold.

Figure 8 reveals that the incidence of $\tau_{912} \geq 2$ LLS increases monotonically for $z > 3.5$. Following previous work, we have modeled the redshift evolution in $\ell_{\tau \geq 2}(z)$ as a power-law with the functional form:

$$\ell_{\tau \geq 2}(z) = C_{\text{LLS}} \left[\frac{1+z}{1+z_*} \right]^{\gamma_{\text{LLS}}} \quad (11)$$

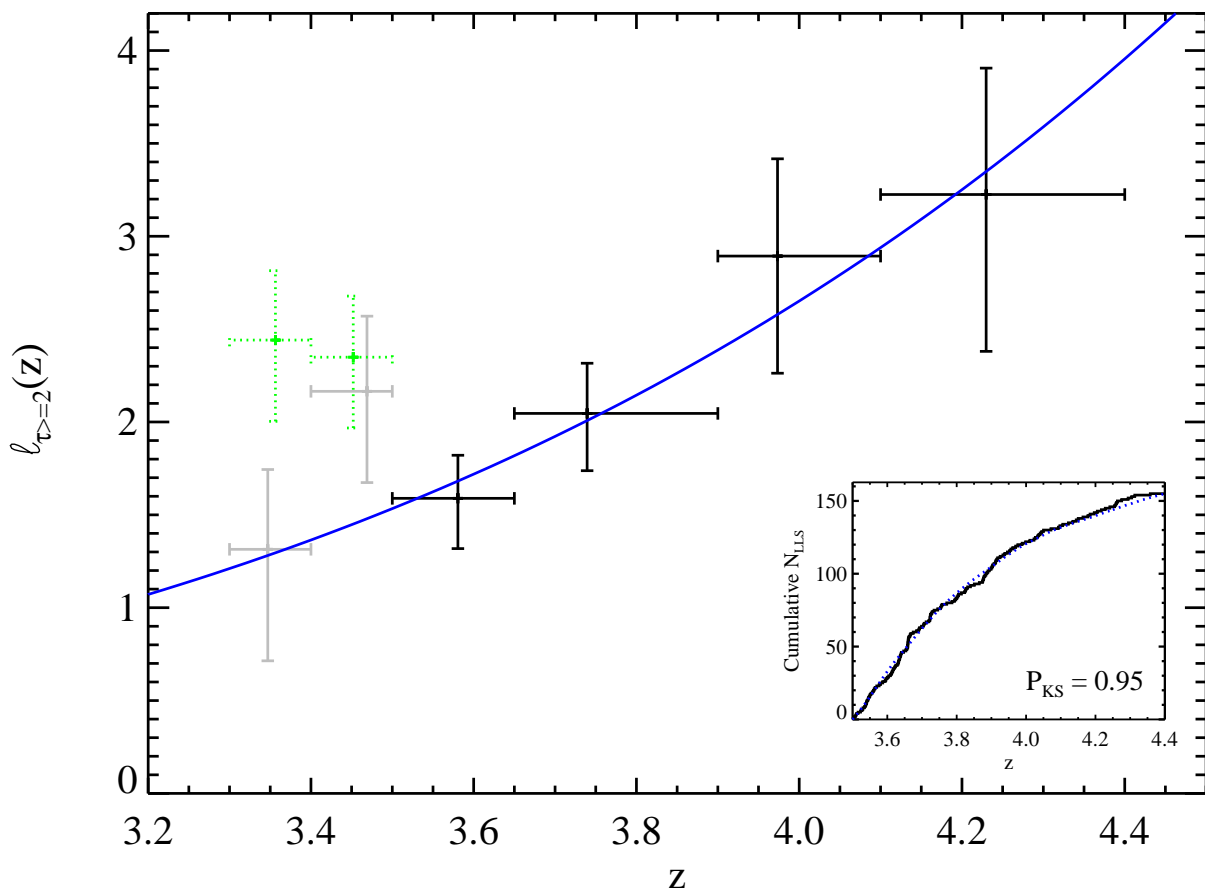


FIG. 8.— Incidence of intervening LLSs with $\tau_{912} \geq 2$ $\ell_{\tau \geq 2}(z)$ as a function of redshift (solid points). Only the darker points were included in a maximum likelihood analysis to determine best-fit power-law (blue curve): $\ell_{\tau \geq 2}(z) = C_{\text{LLS}}[(1+z)/(1+z_*)]^{\gamma_{\text{LLS}}}$, with $z_* \equiv 3.7$, $C_{\text{LLS}} = 1.9 \pm 0.2$, and $\gamma_{\text{LLS}} = 5.2 \pm 1.5$ (68% c.l.). The dotted points, meanwhile, show $\ell_{\tau \geq 2}(z)$ when one includes quasars with $3.4 \leq z_{\text{em}} \leq 3.6$. These measurements are significantly biased to higher values by the SDSS quasar-targeting criteria (PWO09). In the subpanel, the black (solid) curve shows the cumulative number of $\tau_{912} \geq 2$ LLSs detected in our survey of the SDSS-DR7 database adopting the $S/N_{912}^A=2$ threshold. The blue (dotted) curve shows the predicted number of LLSs assuming the best-fit power-law from Figure 8 and adopting the $g(z)$ function from Figure 4. A one-sided KS-test does not rule out the null hypothesis that the model distribution is statistically different from the observations.

setting $z_* \equiv 3.7$. Using standard maximum likelihood techniques (e.g. Storrie-Lombardi et al. 1994), we find best-fit values to the data at $z \geq 3.5$ of $C_{\text{LLS}} = 1.9 \pm 0.2$ and $\gamma_{\text{LLS}} = 5.2 \pm 1.5$ (68% c.l.). The best-fit model is overplotted on the data in Figure 8. The relatively large uncertainty in γ_{LLS} is due to the small redshift interval covered by our survey. Nevertheless, we conclude at high confidence ($> 95\%$) that $\ell_{\tau \geq 2}(z)$ is increasing at least as steeply as $\gamma_{\text{LLS}} = 2$ at $z > 3.5$.

The sub-panel of Figure 8 compares the cumulative number of LLSs detected in the survey against redshift both as observed (solid) and as predicted (dotted) by the best-fit power-law model. For the latter, we adopt the $g(z)$ curves for $S/N_{912}^A=2$ from Figure 4. A one-sided Kolmogorov-Smirnov test yields a probability $P_{\text{KS}} = 0.95$ that the observed distribution is drawn from the adopted power-law expression; the power-law model is a good description of the observations. We comment, however, that the best-fit slope ($\gamma_{\text{LLS}} = 5.2$) is considerably steeper than most previous estimates for the LLSs at this redshift (see § 9.1) and also steeper than the redshift evolution measured for the Ly α forest and damped Ly α systems (Kim et al. 2001; Prochaska et al. 2008). It

is our expectation that γ_{LLS} is likely lower than the central value of our analysis. This assertion will be tested with future observations at $z < 3$ and $z > 4.5$.

For $z < 3.5$, Figure 8 shows two evaluations of $\ell_{\tau \geq 2}(z)$. The light, solid points show the $\ell_{\tau \geq 2}(z)$ values derived from our statistical quasar sample with the restriction that $z_{\text{em}} \geq 3.6$. These values are consistent with an extrapolation of the best-fit power-law. The dotted points in the figure, meanwhile, show the values of $\ell_{\tau \geq 2}(z)$ when one also surveys quasars with $3.4 \leq z_{\text{em}} \leq 3.6$. In this case, we find systematically higher $\ell_{\tau \geq 2}(z)$ values which would indicate a non-physical, non-monotonic evolution in $\ell_{\tau \geq 2}(z)$. These results confirm the findings of PWO09 that the SDSS targeting criteria for quasar spectroscopy biases the sample against sightlines *without* a LLS. The values of $\ell_{\tau \geq 2}(z)$ reported in Table 4, therefore, are restricted to quasars with $z_{\text{em}} \geq 3.6$.

8.2. The Incidence of LLSs in Λ CDM

If one introduces a cosmological model, the observed incidence of $\tau_{912} \geq 2$ LLSs with redshift $\ell_{\tau \geq 2}(z)$ may be translated into physical quantities. Consider first, Δr_{LLS} , the average distance that a photon travels be-

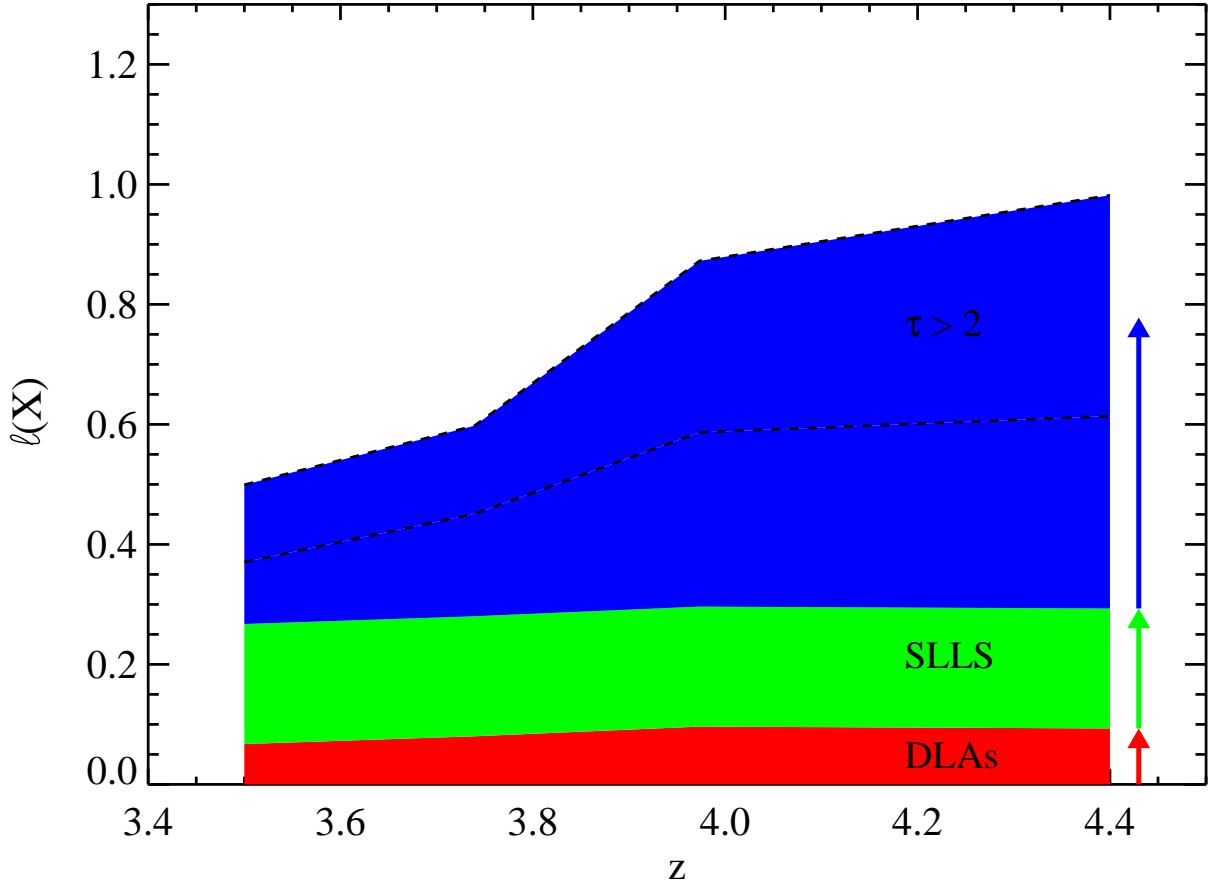


FIG. 9.— Incidence of $\tau_{912} \geq 2$ LLSs as a function of absorption path X as a function of redshift, indicated by the dashed lines. We measure a decrease of ≈ 2 in $\ell_{\tau \geq 2}(X)$ from $z = 4.4$ to 3.5. The widths of the two lower bands (blue, red) indicate estimates of $\ell(X)$ for DLAs and SLLSs (O’Meara et al. 2007; Prochaska & Wolfe 2009); see the text for details. These bands are plotted on top of one another to indicate their total contribution to $\ell_{\tau \geq 2}(X)$ (as indicated by the vertical arrows on the right-hand side of the figure). The (top) blue band, therefore, represents the estimate to $\ell_{\tau \geq 2}(X)$ from LLSs with $N_{\text{HI}} = 10^{17.5} - 10^{19} \text{ cm}^{-2}$. Given the low absolute value and weak evolution in $\ell(X)$ for the SLLSs and DLAs, the evolution in $\ell(X)$ for the LLSs is likely dominated by systems with $\tau_{912} \lesssim 10$.

fore encountering an LLS with $\tau_{912} \geq 2$. Specifically, we define

$$\Delta r_{\text{LLS}} \equiv \ell_{\tau \geq 2}(z)^{-1} \frac{dr}{dz}, \quad (12)$$

where

$$\frac{dr}{dz} = \frac{c}{(1+z)H(z)} \quad (13)$$

and

$$H(z) = H_0 [\Omega_\Lambda + (1+z)^3 \Omega_m]^{1/2}. \quad (14)$$

With our adopted cosmology, we estimate that Δr_{LLS} ranges from ≈ 100 to $40 h_{72}^{-1} \text{ Mpc}$ proper distance from $z = 3.5$ to $z = 4.4$ (Table 4). This is an order of magnitude or more larger than the separation of high z quasars (several Mpc for $L_B \geq 10^{40} \text{ erg s}^{-1} \text{ Hz}^{-1}$; Faucher-Giguere et al. 2009).

An especially informative quantity for associating LLSs to structures in the Universe (e.g. galaxies, filaments) is $\ell(X)$ the number of systems per absorption length (Bahcall & Peebles 1969), where $\ell(X)dX = \ell(z)dz$ and

$$dX = \frac{H_0}{H(z)} (1+z)^2 dz. \quad (15)$$

The quantity $\ell_{\tau \geq 2}(X)$ is defined to remain constant if n_{LLS} , the comoving number density of structures giving rise to a $\tau_{912} \geq 2$ LLS, times σ_{LLS} , the average physical size of the structure remains constant, i.e. $\ell_{\tau \geq 2}(X) \propto n_{\text{LLS}} \sigma_{\text{LLS}}$. Figure 9 presents the evolution of $\ell_{\tau \geq 2}(X)$ for our cosmology as a function of redshift (see also Table 4). We observe a rise in $\ell_{\tau \geq 2}(X)$ with redshift of roughly two times over the $\approx 1 \text{ Gyr}$ from $z = 3.3$ to 4.4. At 99% confidence, we infer an increase in $\ell_{\tau \geq 2}(X)$ over this redshift interval. This follows, of course, from the very steep redshift evolution observed for $\ell_{\tau \geq 2}(z)$ (§ 8.1); in a flat cosmology with Ω_m on the order of Ω_Λ , an $\ell_{\tau \geq 2}(z)$ evolution steeper than $(1+z)^{1/2}$ implies $\ell_{\tau \geq 2}(X)$ is also increasing. We conclude that n_{LLS} and/or σ_{LLS} are increasing with redshift at $z \approx 3.5$. We discuss the implications of this result in § 9.4.

8.3. $f(N_{\text{HI}}, X)$ at $z \approx 3.7$

In this subsection, we combine our results with previous work on the IGM to place constraints on the H I frequency distribution, $f(N_{\text{HI}}, X)$. We focus this analysis at a single redshift ($z = 3.7$) where our observations have greatest statistical power.

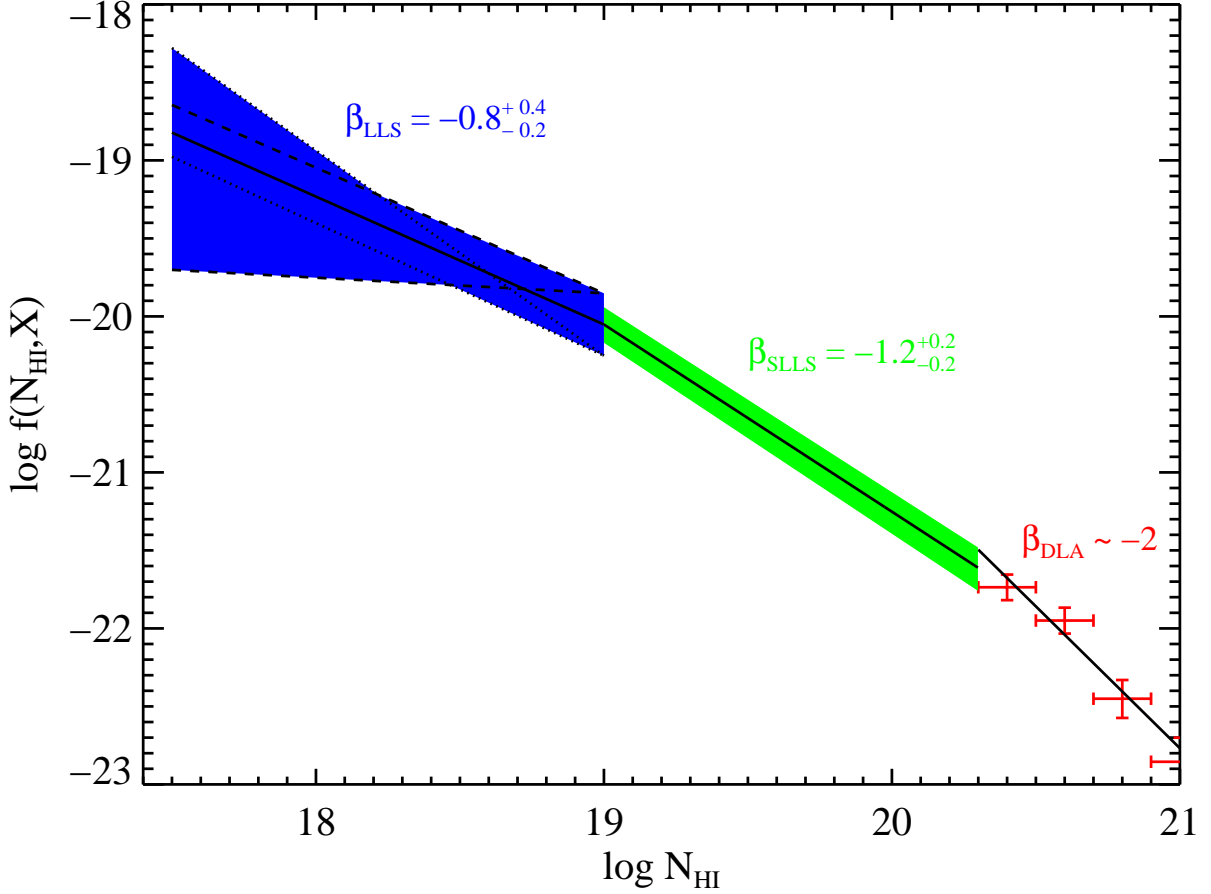


FIG. 10.— The N_{HI} frequency distribution $f(N_{\text{HI}}, X)$ observed for the SLLSs (green, $N_{\text{HI}} = 10^{19} - 10^{20.3} \text{ cm}^{-2}$; O’Meara et al. 2007) and DLAs (red, $N_{\text{HI}} \geq 10^{20.3} \text{ cm}^{-2}$; Prochaska & Wolfe 2009). The blue band is an estimate of $f(N_{\text{HI}}, X)$ for LLSs having $N_{\text{HI}} = 10^{17.5} - 10^{19} \text{ cm}^{-2}$ under the assumptions of a power-law form ($f(N_{\text{HI}}, X) \propto N_{\text{HI}}^{\beta_{\text{LLS}}}$) and constrained by the observed incidence of SLLSs and $\tau \geq 2$ LLS (this paper). We find $\beta_{\text{LLS}} = -0.8^{+0.4}_{-0.2}$ (68% c.l.) for conservative estimates on the value of $f(N_{\text{HI}}, X)$ at 10^{19} cm^{-2} and allowing for 20% uncertainty in $\ell_{\tau \geq 2}(X)$. The dashed and dotted curves indicate the range of power-laws that satisfy the observations.

8.3.1. $f_{\text{LLS}}(N_{\text{HI}}, X)$

Although our observations and LLS analysis are insensitive to the H I column densities of the LLSs, they do provide an integral constraint on the frequency distribution of N_{HI} , $f(N_{\text{HI}}, X)$. We constrain the N_{HI} frequency distribution of $\tau_{912} \lesssim 10$ LLS per absorption length, $f_{\text{LLS}}(N_{\text{HI}}, X)$, at column densities $N_{\text{HI}} = 10^{17.5} - 10^{19} \text{ cm}^{-2}$ as follows. Previous surveys at $z > 3$ have measured $f(N_{\text{HI}}, X)$ for column densities $N_{\text{HI}} \geq 10^{19} \text{ cm}^{-2}$ (Prochaska et al. 2005; O’Meara et al. 2007; Prochaska & Wolfe 2009; Noterdaeme et al. 2009; Guimaraes et al. 2009). These authors have parameterized the distribution functions as single (SLLSs) and double (DLAs) power-laws of the following form:

$$f_{\text{SLLS}}(10^{19} \text{ cm}^{-2} \leq N_{\text{HI}} < 10^{20.3} \text{ cm}^{-2}, X) = k_{\text{SLLS}} N_{\text{HI}}^{\beta_{\text{SLLS}}} \quad (16)$$

and

$$f_{\text{DLA}}(N_{\text{HI}} \geq 10^{20.3} \text{ cm}^{-2}, X) = k_{\text{DLA}} \left(\frac{N_{\text{HI}}}{N_d} \right)^{\beta_{\text{DLA}}} \quad (17)$$

$$\text{where } \beta_{\text{DLA}} = \begin{cases} \beta_3 : N_{\text{HI}} < N_d; \\ \beta_4 : N_{\text{HI}} \geq N_d \end{cases} \quad (17)$$

Figure 10 presents these frequency distributions. For the SLLSs at $z = 3.7$, we have taken $\beta_{\text{SLLS}} = -1.2 \pm 0.2$ and normalized the power-law by taking

$$\ell_{\text{SLLS}}(X) = \int_{10^{19} \text{ cm}^{-2}}^{10^{20.3} \text{ cm}^{-2}} f_{\text{SLLS}}(N_{\text{HI}}, X) dN_{\text{HI}} = 0.2 \quad (18)$$

These values are consistent with the range of published measurements at this redshift (Péroux et al. 2005; O’Meara et al. 2007; Guimaraes et al. 2009). For the DLAs, we have evaluated $f_{\text{DLA}}(N_{\text{HI}}, X)$ from the SDSS-DR5 (Prochaska & Wolfe 2009) over the redshift interval $z = [3.4, 4.0]$, giving $N_d = 10^{21.75}$, $\beta_3 = -1.8$, $\beta_4 < -3$, and $k_{\text{DLA}} = 7 \times 10^{-25} \text{ cm}^2$.

We estimate $f(N_{\text{HI}}, X)$ for the interval $N_{\text{HI}} = [10^{17.5}, 10^{19}] \text{ cm}^{-2}$, which we refer to as $f_{\text{LLS}}(N_{\text{HI}}, X)$, under the following assumptions/constraints: (i) $f_{\text{LLS}}(N_{\text{HI}}, X)$ has a power-law form

$$f_{\text{LLS}}(N_{\text{HI}}, X) = k_{\text{LLS}} N_{\text{HI}}^{\beta_{\text{LLS}}} \quad (19)$$

and (ii) $f_{\text{LLS}}(N_{\text{HI}}, X)$ at $N_{\text{HI}} = 10^{19} \text{ cm}^{-2}$ is consistent with the range of values given by the SLLSs. Specifically,

we demand $\log f(N_{\text{HI}} = 10^{19} \text{ cm}^{-2}, X) = -20.05 \pm 0.2$; (iii) we impose the integral constraint based on the the observed incidence of $\tau_{912} \geq 2$ LLSs:

$$\ell_{\tau \geq 2}(X) = \int_{10^{17.5} \text{ cm}^{-2}}^{\infty} f(N_{\text{HI}}, X) dN_{\text{HI}} \quad (20)$$

At $z \approx 3.7$, we estimate $\ell_{\tau \geq 2}(X) = 0.5 \pm 0.1$ (Figure 9).

Overplotted on Figure 10 are the power-law frequency distributions (shown as dashed, dotted and a solid line) that satisfy the extrema of those constraints. The shaded region shows the intersection of the curves and roughly represents the allowed region of $f(N_{\text{HI}}, X)$ values. We find $\beta_{\text{LLS}} = -0.8 \pm 0.3$, and derive $k_{\text{LLS}} = 10^{-4.5} \text{ cm}^2$ for the central value. Table 5 further summarizes these results.

Our analysis reveals that $f(N_{\text{HI}}, X)$ becomes increasingly shallow with decreasing N_{HI} . Only for the most extreme values of our analysis, low $f(N_{\text{HI}}, X)$ at $N_{\text{HI}} = 10^{19} \text{ cm}^{-2}$ and a large $\ell_{\tau \geq 2}(z)$ value, do we recover $\beta_{\text{LLS}} < -1$. This flattening of $f(N_{\text{HI}}, X)$ was suggested by previous authors based on a similar analysis but with much poorer observational constraints on $\ell_{\tau \geq 2}(X)$ (Péroux et al. 2003; Prochaska et al. 2005; O’Meara et al. 2007). Remarkably, our results indicate $\beta_{\text{LLS}} > -1$ which means that the IGM has a *higher* total covering fraction per unit pathlength for sightlines with $N_{\text{HI}} = 10^{19} \text{ cm}^{-2}$ than those with $N_{\text{HI}} = 10^{18} \text{ cm}^{-2}$.

8.3.2. Constraints from Measurements of the Mean Free Path

Traditionally, the mean free path to ionizing radiation in the IGM ($\lambda_{\text{mfp}}^{912}$) has been estimated from the observed incidence of LLSs (e.g. Meiksin & Madau 1993). Recently, PWO09 introduced a new approach to measure $\lambda_{\text{mfp}}^{912}$ from stacked quasar spectra, without any consideration of LLSs. We can reverse the problem, therefore, and use the $\lambda_{\text{mfp}}^{912}$ results to constrain properties of $f(N_{\text{HI}}, X)$. One expects to have the greatest sensitivity to absorption systems with $\tau_{912} \approx 1$, i.e. the LLSs and partial LLSs.

At $z = 3.7$, PWO09 estimate $\lambda_{\text{mfp}}^{912} = 47h_{72}^{-1} \text{ Mpc}$ proper distance. This means that in the absence of an expanding universe, a packet of 1 Ryd photons at $z = 3.7$ would be attenuated by $\exp(-1)$ after traveling $\lambda_{\text{mfp}}^{912}$. One can also express the mean free path as an opacity, $\kappa_{912} = 1/\lambda_{\text{mfp}}^{912}$, which can be related to the optical depth of a 1 Ryd photon as:

$$\kappa_{912} = \frac{d\tau_{\text{eff}}^{912}}{dr} = \frac{d\tau_{\text{eff}}^{912}}{dz} \frac{dz}{dr}. \quad (21)$$

Finally, we can relate the differential optical depth to the H I frequency distribution of absorbers:

$$\frac{d\tau_{\text{eff}}^{912}(z)}{dz} = \int_{N_{\text{HI}}^{\text{min}}}^{\infty} f(N_{\text{HI}}, z) \{1 - \exp[-N_{\text{HI}}\sigma_{\text{ph}}^{912}]\} dN_{\text{HI}} \quad (22)$$

with σ_{ph}^{912} the photoionization cross-section evaluated at 1 Ryd and dr/dz given by Equation 13. Although the integral should be evaluated with $N_{\text{HI}}^{\text{min}} = 0$, in practice

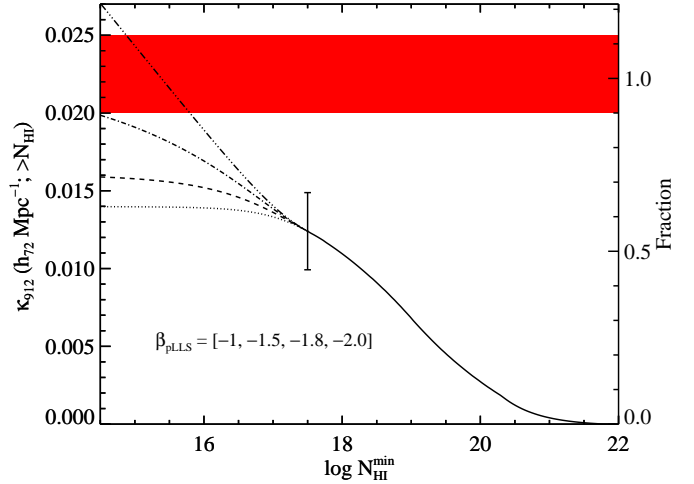


FIG. 11.— This figure shows the opacity at the Lyman limit κ_{912} contributed by absorbers with $N_{\text{HI}} \geq N_{\text{HI}}^{\text{min}}$. For $N_{\text{HI}}^{\text{min}} \geq 10^{17.5} \text{ cm}^{-2}$ (solid curve), which corresponds to our LLS survey, we have adopted the estimate of $f(N_{\text{HI}}, X)$ from Figure 10 in the calculation. We estimate a 20% uncertainty in the contribution of LLSs to κ_{912} , as shown in the figure. For $N_{\text{HI}}^{\text{min}} < 10^{17.5} \text{ cm}^{-2}$, we assume $f(N_{\text{HI}}, X)$ follows a simple power-law with exponent β_{pLLS} , and show a series of extrapolations (dash and dotted curves). The solid (red) horizontal band centered at $\kappa_{912} = 0.0225 h_{72} \text{ Mpc}^{-1}$ indicates the measurement at $z \approx 3.7$ by PWO09. These results imply that LLSs contribute $\approx 55\%$ of the mean free path ($\approx 33\%$ for systems with $\tau_{912} \gg 1$) and that β_{pLLS} must be steeper than ≈ -1.5 to explain all of these observations.

$d\tau_{\text{eff}}^{912}$ is insensitive to the minimum N_{HI} column density for any value $N_{\text{HI}}^{\text{min}} \leq 10^{12} \text{ cm}^{-2}$.

Figure 11 shows the κ_{912} value at $z = 3.7$ from PWO09 as a horizontal band that illustrates the 1σ error interval. The solid curve, meanwhile, corresponds to the evaluation of Equation 21 using our best estimation of $f(N_{\text{HI}}, X)$ (Figure 10) as a cumulative function of $N_{\text{HI}}^{\text{min}}$. At the limiting N_{HI} value of our LLS survey ($10^{17.5} \text{ cm}^{-2}$), we estimate that $\approx 55\%$ of the opacity to ionizing radiation is contributed by $\tau_{912} \geq 2$ LLSs. The uncertainty in the results is roughly proportional to the uncertainty in $\ell_{\tau \geq 2}(z)$, i.e. $\approx 20\%$ as indicated by the error bars on the figure. It is notable that $\approx 1/3$ of the contribution to κ_{912} is from very optically thick absorbers ($\tau_{912} \gg 1$), i.e. the SLLSs and DLAs.

It is also evident from Figure 11 that systems with $\tau_{912} \leq 2$ must contribute to κ_{912} . For $N_{\text{HI}}^{\text{min}} < 10^{17.5} \text{ cm}^{-2}$, we continue the calculation by assuming that $f(N_{\text{HI}}, X)$ follows a power-law

$$f_{\text{pLLS}}(N_{\text{HI}} < 10^{17.5} \text{ cm}^{-2}, X) = k_{\text{pLLS}} N_{\text{HI}}^{\beta_{\text{pLLS}}} \quad (23)$$

constrained to match $f_{\text{LLS}}(N_{\text{HI}}, X)$ at $N_{\text{HI}} = 10^{17.5} \text{ cm}^{-2}$. We find that models with $\beta_{\text{pLLS}} \geq -1.8$ cannot reproduce the $\lambda_{\text{mfp}}^{912}$ results. In fact, the data favor $\beta_{\text{pLLS}} \approx -2$ i.e. a much steeper power-law than inferred for the LLS and also than that commonly observed for the Ly α forest. These conclusions depend rather insensitively on our estimate of $\ell_{\tau \geq 2}(X)$; slopes only as shallow as -1.7 are allowed if we adopt our highest estimates for $\ell_{\tau \geq 2}(X)$.

Thus far, these inferences on $f(N_{\text{HI}}, X)$ for absorption systems with $\tau_{912} < 2$ have ignored observations of the Ly α forest. By including these data, we provide

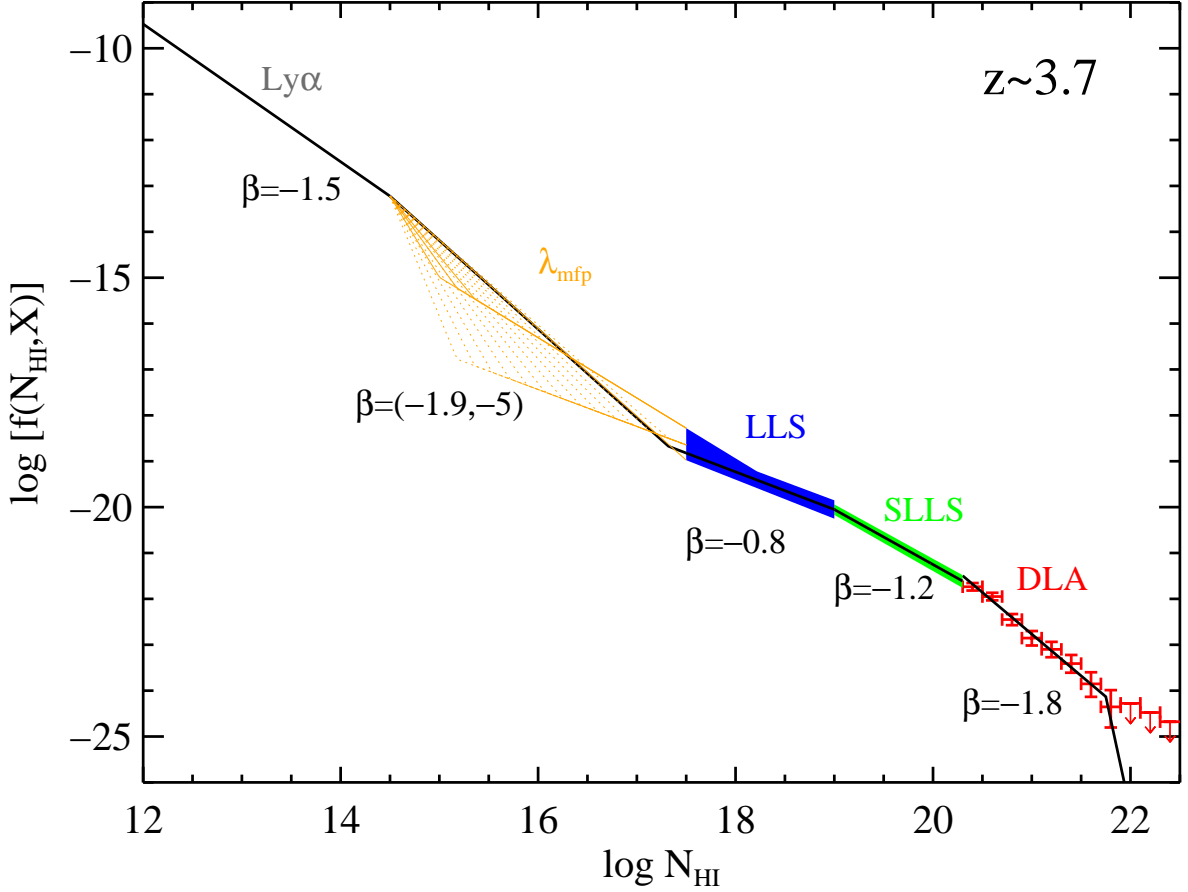


FIG. 12.— The solid black curve shows our estimation of $f(N_{\text{HI}}, X)$ at $z \approx 3.7$ as a series of six power-laws that intersect at $N_{\text{HI}} = [10^{14.5}, N_{\text{pLLS}}, 10^{19.0}, 10^{20.3}, 10^{21.75}] \text{ cm}^{-2}$, where N_{pLLS} is constrained to lie between $N_{\text{HI}} = 10^{15} - 10^{17.5} \text{ cm}^{-2}$. The observational constraints for $f(N_{\text{HI}}, X)$ at $N_{\text{HI}} \geq 10^{19} \text{ cm}^{-2}$ are as in Figure 10. The results here also include constraints from the observed mean free path (PWO09) and the effective Ly α opacity of the Ly α forest (Faucher-Giguère et al. 2008b). The orange curves show the regions of $f(N_{\text{HI}}, X)$ that reproduce the mean free path measurement and also connect to the Ly α forest at $N_{\text{HI}} = 10^{14.5} \text{ cm}^{-2}$.

further constraints on $f(N_{\text{HI}}, X)$ for $N_{\text{HI}} = 10^{15} \text{ cm}^{-2}$ to 10^{19} cm^{-2} . To derive these constraints, however, we must adopt a functional form for $f(N_{\text{HI}}, X)$. Absent a physical model, we take an empirical approach. We express $f(N_{\text{HI}}, X)$ as a series of six power-laws that intersect at $N_{\text{HI}} = [10^{14.5}, N_{\text{pLLS}}, 10^{19.0}, 10^{20.3}, 10^{21.75}] \text{ cm}^{-2}$, where N_{pLLS} is constrained to lie between $N_{\text{HI}} = 10^{15} - 10^{17.5} \text{ cm}^{-2}$. Other than a small ‘kink’ at $N_{\text{HI}} = 10^{20.3} \text{ cm}^{-2}$, the power-laws are required to match at each intersection point.

The power laws are forced to satisfy the following observational constraints:

1. The power-laws for $N_{\text{HI}} \geq 10^{17.5}$ are constrained as described at the start of this sub-section.
2. For the Ly α forest, we assume $f(N_{\text{HI}}, X) \propto N_{\text{HI}}^{-1.5}$ and normalize at $z = 3.7$ by the effective Ly α optical depth $\tau_{\text{eff}}^{\alpha}$ measured by Faucher-Giguère et al. (2008b) assuming a b -value distribution $f(b) \propto b^{-5} \exp[-b^4/b^4]$ (Hui & Rutledge 1999).
3. The integrated opacity of the IGM at the Lyman limit is constrained by the measurement of PWO09, i.e. $\lambda_{\text{mfp}}^{912} = 47h_{72}^{-1} \text{ Mpc}$.

For the range of power-laws derived from our analysis of the LLS results (Figure 10), we show in Figure 12 the range of $f(N_{\text{HI}}, X)$ distributions that also satisfy all of the constraints. We find viable models with N_{pLLS} values that range across the allowed interval. These are correlated with β_{pLLS} values ranging from $\beta_{\text{pLLS}} = -1.9$ to -5 (Table 5).

The principal results of this analysis are threefold. First, the single power-law connecting the Ly α forest to the SLLS satisfies neither the LLS nor mean free path constraints. There is at least one break between $N_{\text{HI}} = 10^{14.5} \text{ cm}^{-2}$ and $N_{\text{HI}} = 10^{19} \text{ cm}^{-2}$ where $f(N_{\text{HI}}, X)$ steepens to $\beta < -1.8$ and then flattens to $\beta \approx -1$. This is consistent with conclusions drawn from line-counting statistics of Ly α forest lines (e.g. Petitjean et al. 1993; Kim et al. 2002). Second, the added $\lambda_{\text{mfp}}^{912}$ and Ly α forest constraints rule out the lowest values of $f_{\text{LLS}}(N_{\text{HI}}, X)$ at $N_{\text{HI}} \approx 10^{17.5} \text{ cm}^{-2}$ that were otherwise allowed by our LLS results. Specifically, the data require $\log f(N_{\text{HI}} = 10^{17} \text{ cm}^{-2}, X) \geq -19$ and the (blue) shaded region in Figure 12 shows the proper allowed range for $f_{\text{LLS}}(N_{\text{HI}}, X)$. Finally, we find that the slope of $f(N_{\text{HI}}, X)$ must steepen to $\beta_{\text{pLLS}} \leq -1.8$ at columns $N_{\text{HI}} \gtrsim 10^{14.5} \text{ cm}^{-2}$.

TABLE 5
SUMMARY OF $f(N_{\text{HI}}, X)$ RESULTS

$\ell_{\text{LLS}}(z)^a$	$\log f_{19}^b$	β_{LLS}	$\log k_{\text{LLS}}$	$\log N_{\text{pLLS}}^c$	β_{pLLS}
Preferred Values					
0.23	-20.05	-0.8	-4.5	17.3	-1.9
Conservative Range of Allowed Values					
0.23	-20.05	-0.8	-4.5	17.1	-2.0
				17.3	-1.9
				17.5	-1.9
0.15	-20.25	-0.9	-4.1	17.5	-1.9
0.35	-20.25	-1.3	4.7	15.0	-3.5
				15.2	-3.0
				15.4	-2.6
0.15	-19.85	-0.1	-18.0
0.35	-19.85	-0.8	-4.6	15.2	-5.2
				15.4	-4.3
				15.5	-3.7
				15.7	-3.3
				15.9	-3.0
				16.1	-2.7
				16.2	-2.5
				16.4	-2.4
				16.6	-2.2
				16.8	-2.1
				17.0	-2.0
				17.1	-1.9
				17.3	-1.9

NOTE. — The analysis throughout assumes that the DLAs contribute $\ell(X) = 0.09$ to $\ell_{\tau \geq 2}(X)$.

^aThe incidence of $\tau_{912} \geq 2$ LLS $\ell_{\tau \geq 2}(X)$, attributed to LLS with $N_{\text{HI}} < 10^{19} \text{ cm}^{-2}$.

^bThe adopted value of $f(N_{\text{HI}}, X)$ at $N_{\text{HI}} = 10^{19} \text{ cm}^{-2}$.

^cThe break column density within the Ly α forest as defined in the text. Entries without values have power-law descriptions for the LLS that cannot satisfy the mean free path and Ly α forest constraints.

8.4. The Incidence of Proximate LLSs (PLLSs)

The results presented thus far all refer to intervening LLSs, i.e., systems restricted to have z_{LLS} blueward of 3000 km s^{-1} from the quasar emission redshift. This restriction was imposed to isolate the ‘ambient’ IGM and avoid biases related to having performed the search for bright, background quasars. In the space surrounding a bright quasar, one predicts at least two such biases: (1) bright, high z quasars are known to cluster strongly ($r_0 > 15 h^{-1} \text{ Mpc}$; Shen et al. 2007) suggesting these objects trace massive structures in the young universe. The local environment of bright quasars, therefore, has an uncommonly high density (at least in dark matter) which may give a higher incidence of LLSs; (2) the radiation field of the quasar will ionize gas to large distances, reducing the incidence of LLSs. For damped Ly α systems, the first effect dominates as one observes an enhanced rate of proximate DLAs (PDLAs) relative to the intervening systems (Russell et al. 2006; Prochaska et al. 2008).

Following the formalism presented in Prochaska et al. (2008), we have estimated the incidence of PLLSs in a series of redshift intervals. First, we re-measured the quasar emission redshifts for all systems with $S/N_{912}^A \geq 2$ at the Lyman limit and with a $\tau_{912} \geq 2$ LLS within 5000 km s^{-1} of z_{em} . The SDSS quasar redshifts reported in the standard DR7 data release are known to have sig-

TABLE 6
SDSS-DR7 PROXIMATE $\tau_{912} \geq 2$
LLS SURVEY

Quasar	z_{em}	z_{LLS}
J001115.23+144601.8	4.967	...
J001820.71+141851.5	3.936	...
J004219.74-102009.4	3.880	...
J004240.65+141529.6	3.687	3.684
J010619.24+004823.3	4.449	...
J011351.96-093551.0	3.668	...
J012403.77+004432.7	3.834	...
J014049.18-083942.5	3.713	3.693
J015048.82+004126.2	3.702	...
J015339.61-001104.8	4.194	...
J021318.98-090458.3	3.794	3.797
J022518.35-001332.2	3.628	...
J024447.78-081606.1	4.068	...
J025518.58+004847.6	3.989	...
J031213.97-062658.8	4.031	...
J034402.85-065300.6	3.957	...
J073149.50+285448.6	3.676	...
J074154.59+341252.1	3.905	...
J074500.47+341731.1	3.713	...
J074640.16+344624.7	4.010	...
J074711.15+273903.3	4.154	...
J075006.62+491834.1	3.603	...
J075017.49+405825.3	3.864	3.849
J075103.95+424211.6	4.163	...
J075347.41+281805.2	4.031	...
J075552.41+134551.1	3.673	...
J075732.89+441424.6	4.170	...

NOTE. — [The complete version of this table is in the electronic edition of the Journal. The printed edition contains only a sample.]

nificant systematic errors. Following the prescriptions described in Shen et al. (2007), J. Hennawi has kindly remeasured the redshifts for all of the quasars. Second, we analyzed the quasars whose absorbed continuum at the wavelength of the Lyman limit corresponding to 3000 km s^{-1} blueward of z_{em} is twice the median-smoothed, 1σ error-array. This establishes the survey path. All PLLSs identified redward of this 3000 km s^{-1} offset form the statistical sample (Table 6). The incidence, $\ell_{\text{PLLS}}(z)$, is then estimated in arbitrary redshift intervals assuming the same estimator for intervening LLSs (Equation 10). These results are presented in Figure 13 and compared against the incidence of intervening LLSs.

Ignoring the data at $z < 3.6$ (which we suspect to be biased high by the SDSS targeting criteria; PWO09), the incidence of PLLSs roughly tracks that of intervening LLSs but is $\approx 25\%$ lower than the intervening systems. The inset figure shows the observed cumulative number of PLLSs (dark curve) versus the predicted number (light curve) assuming the best-fit power-law for $\ell_{\tau \geq 2}(z)$ of intervening LLSs. A one-sided KS test yields only a 1% probability that the two distributions are drawn from the same parent population. We also remind the reader that corrections for the blending bias described in § 7.4 will likely reduce $\ell_{\text{PLLS}}(z)$ further, especially at $z \sim 4$. The principal implication is that $\tau_{912} \geq 2$ LLSs toward $i < 20 \text{ mag}$ quasars at $z > 3.5$ suffer from a proximity effect, presumably due to the ionizing radiation field of the quasar itself. Given the observed enhancement of strong LLSs at $z \approx z_{\text{em}}$ along sightlines *transverse* to such quasars, our results lend further evidence that

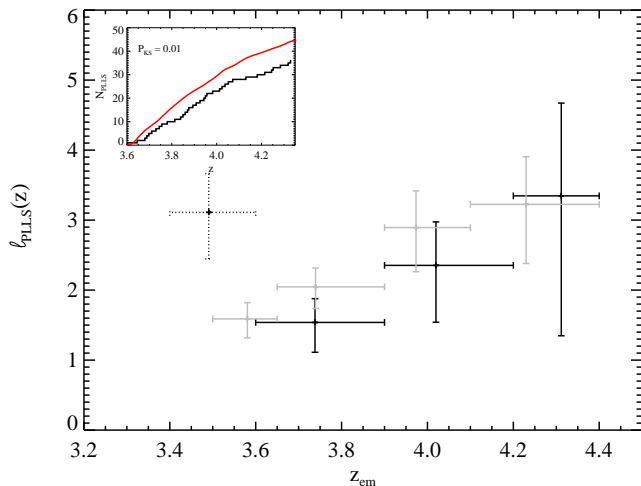


FIG. 13.— The solid and dark points show the incidence $\ell_{\text{PLLs}}(z)$ of proximate LLSs (PLLs; LLSs with $\tau_{912} \geq 2$ that occur within 3000 km s^{-1} of the background quasar) per unit redshift against quasar emission redshift. These are compared against the same quantity for intervening LLSs (gray points). The data point at $z_{\text{em}} < 3.6$ has been dotted out because it is biased by the SDSS targeting criteria (PWO09). Ignoring that last point, we find that the incidence of PLLs roughly follows that of intervening systems but is systematically lower by $\approx 25\%$ at $z < 4$. The inset figure shows the cumulative number of PLLs observed (black curve) against the predicted number using the power-law model for $\ell_{\tau \geq 2}(z)$ (§ 8.1) and the $g(z)$ curve for PLLs (Figure 4).

quasar emission at $\approx 1 \text{ Ryd}$ is usually anisotropic (Henawi & Prochaska 2007).

Before concluding this section, we comment that the PLLS analysis is subject to another systematic error. In performing our LLS survey, we have identified and removed all quasars with very strong associated absorption, e.g. BALs. The intent of this procedure was to remove the signatures of absorption from gas very local ($< 1 \text{ kpc}$) to the quasar from the analysis. It is possible, however, that the associated absorption in some of these removed quasars is due to a PLLS at distances $\gg 1 \text{ kpc}$ and not very local gas. This would lead to an underestimate of $\ell_{\text{PLLs}}(z)$. Alternatively, we may not have identified all of the local absorbers and therefore might have overestimated $\ell_{\text{PLLs}}(z)$. In either case, we caution that a systematic error of the order of $10 - 20\%$ should be attributed to this effect.

9. DISCUSSION

9.1. Comparisons with Previous Work

Surveys for Lyman limit systems have been carried out for several decades now (Tytler 1982; Sargent et al. 1989; Lanzetta 1991; Storrie-Lombardi et al. 1994; Stengler-Larrea et al. 1995; Péroux et al. 2003). These have been performed primarily at optical wavelengths on heterogeneous quasar samples drawn from a diverse set of survey approaches: color-selection, radio detection, slitless spectroscopy, etc. The authors adopted differing completeness limits for τ_{912} (ranging from 1 to 3) and used different approaches to establishing the pathlength that establishes $\ell_{\tau \geq 2}(z)$. Little attention was given to assessing systematic error, and several of the effects described in § 7 assuredly apply to the previous works. Perhaps not surprisingly, therefore, most of the previous estimates of $\ell(z)$ are in disagreement with our results.

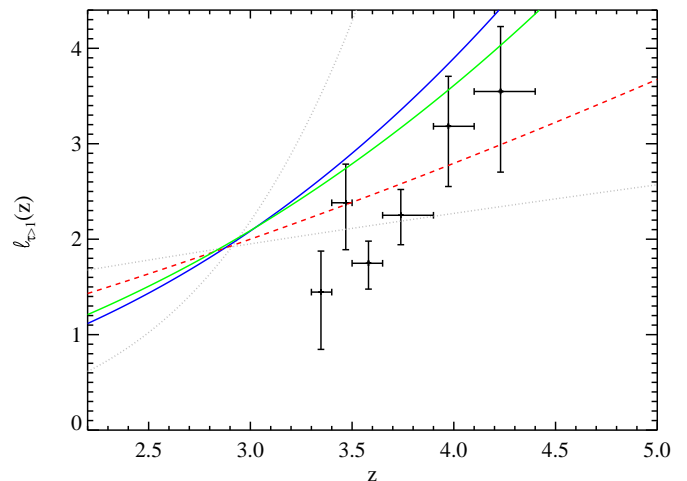


FIG. 14.— Estimates of $\ell_{\tau \geq 1}(z)$ from several previous studies, parameterized as power-laws with the parameters listed in Table 7. The dotted (gray) lines show estimates from Sargent et al. (1989) and Lanzetta (1991). The dashed curve is the estimate from Stengler-Larrea et al. (1995) and the solid blue and green curves are from Storrie-Lombardi et al. (1994) and Péroux et al. (2003) respectively. For the values of our survey, we have increased the $\ell_{\tau \geq 2}(z)$ results by 10% to match the $\tau_{912} = 1$ threshold of the previous work. Our results indicate a significantly lower incidence of LLSs at $z < 4$ than suggested by the previous estimates. This lower incidence is consistent with recent estimates of the mean free path to ionizing radiation (POW09).

TABLE 7
POWER-LAW PARAMETERS OF $\ell_{\tau \geq 1}(z)$

γ_{LLS}	C_{LLS}	Reference
0.68	0.76	Sargent et al. (1989)
5.7	0.00081	Lanzetta (1991)
2.8	0.043	Storrie-Lombardi et al. (1994)
1.5	0.25	Stengler-Larrea et al. (1995)
2.45	0.07	Péroux et al. (2003)

In Figure 14 we present estimates of $\ell(z)$ from several previous studies, parameterized as in Equation 11 (Table 7 lists the parameters). The dotted lines show estimates from Sargent et al. (1989) and Lanzetta (1991), which included very few observations at $z > 3.5$ and had very discrepant guesses for the high z universe. The dashed line shows the result from Stengler-Larrea et al. (1995) who integrated previous work with a new measurement at $z < 1$ and an (still) unpublished survey by Steidel & Sargent. Finally, the solid curves show the results from Storrie-Lombardi et al. (1994) and Péroux et al. (2003) who surveyed LLSs at $z \sim 4$ using color-selected quasars. All of these analyses were claimed to correspond to the incidence of LLSs with $\tau_{912} \geq 1$, $\ell_{\tau \geq 1}(z)$, although a careful review of the literature raises doubts regarding this assertion. Nevertheless, to make comparisons with their reported $\tau_{912} \geq 1$ results we have boosted each of our $\ell_{\tau \geq 2}(z)$ estimations. Formally, we estimate a correction of 6% from our derived $f(N_{\text{HI}}, X)$ distribution but, in practice, we adopt a more conservative 10% correction.

Our results on $\ell_{\tau \geq 1}(z)$ at $z > 4$ are lower than the values derived from the APM surveys, but within $\approx 1\sigma$ of concordance. The more important differences are be-

tween the estimations at $z < 4$. All of the previous work was essentially derived from the surveys of Sargent et al. (1989) and Lanzetta (1991) and, therefore, the curves all intersect at $z \approx 3$ at a $\ell_{\tau \geq 1}(z) \approx 2$. Our results suggest that much of the previous work at $z \sim 3$ overestimated the incidence of LLSs. The original survey by Sargent et al. (1989) is in fair agreement with an extrapolation of our power-law form for $\ell_{\tau \geq 1}(z)$ to $z = 3$, but the re-analysis by Stengler-Larrea et al. (1995) of unpublished spectra taken by Steidel & Sargent led to a higher estimate at this redshift. We suspect that this later work gave $\ell_{\tau \geq 1}(z)$ values that were too high either because of sample variance (i.e. small number statistics), selection bias in the quasar sample, and/or the systematic effects described in § 7.

It is also reasonable to consider whether our SDSS survey has been biased low by an unidentified systematic error. The measurement of $\lambda_{\text{mfp}}^{912}$, however, indicates that this is not the case. Reconsider the analysis presented in § 8.3.2 (Figure 11). If we adopted a 50% higher incidence of $\tau_{912} \geq 2$ LLSs, e.g. $\ell_{\tau \geq 2}(X) = 0.75$ at $z = 3.7$, then we would infer a much steeper slope for the LLSs ($\beta_{\text{LLS}} \approx -1.5$) and then would require a power-law shallower than $\beta = -0.5$ for $N_{\text{HI}} = 10^{15} \text{ cm}^{-2} - 10^{17} \text{ cm}^{-2}$. This would force $f(N_{\text{HI}}, X)$ to steepen to $\beta < -3$ at $N_{\text{HI}} \approx 10^{14.5} \text{ cm}^{-2}$. Such an extreme $f(N_{\text{HI}}, X)$ distribution is non-physical and, more importantly, ruled out by observed line-statistics of the Ly α forest (Kim et al. 2002; Misawa et al. 2007). We conclude that the incidence of LLSs at $z \approx 3.7$ cannot be more than 30% higher than our central value, and, at present, we cannot identify a bias that would lead to such a large systematic underestimate in our results.

9.2. Evolution in $\ell_{\tau \geq 1}(z)$ from $z = 0 - 4$

Previous work has debated whether $\ell_{\tau \geq 1}(z)$ evolves as a single power-law $(1+z)^{\gamma_{\text{LLS}}}$ from $z \approx 0-4$ (e.g. Stengler-Larrea et al. 1995). In § 8.1, we modeled our observations with a single power-law having $\gamma_{\text{LLS}} = 5.2 \pm 1.5$. The observed evolution in the mean free path (PWO09) also suggests a step evolution ($\gamma_{\text{LLS}} > 2$) for the LLSs. We now consider whether a single power-law extrapolation is a good description of $\ell_{\tau \geq 1}(z)$ for $z < 3$.

Survey of other H I absorption systems have demonstrated that a single $(1+z)^\gamma$ power-law is a poor description of the Ly α forest (Weymann et al. 1998) and the damped Ly α systems (Prochaska et al. 2008). In the former case, one observes a flattening in the Ly α line-density at $z \sim 1$ which has been interpreted to result from a corresponding decline in the intensity of the extragalactic UV background (EUVB Weymann et al. 1998; Davé et al. 1999). It is plausible that a similar effect would influence the LLS. In Figure 15, we present estimates of $\ell_{\tau \geq 1}(z)$ at $z \sim 3.5$, estimated by increasing the measured $\ell_{\tau \geq 2}(z)$ values by 10%. These are compared against the $z \sim 1$ measurement from (Stengler-Larrea et al. 1995, see Ribauldo et al., in prep for a new estimate). Overplotted on the data is a solid curve that shows the best-fit power-law to the SDSS results. The dashed curves show 2σ departures from this model, extrapolated to $z = 0$. It is evident that none of these curves intersect the low redshift observations. We conclude, with high confidence, that a strict $(1+z)^{\gamma_{\text{LLS}}}$ power-law does not describe the evolution of $\ell_{\tau \geq 1}(z)$ from

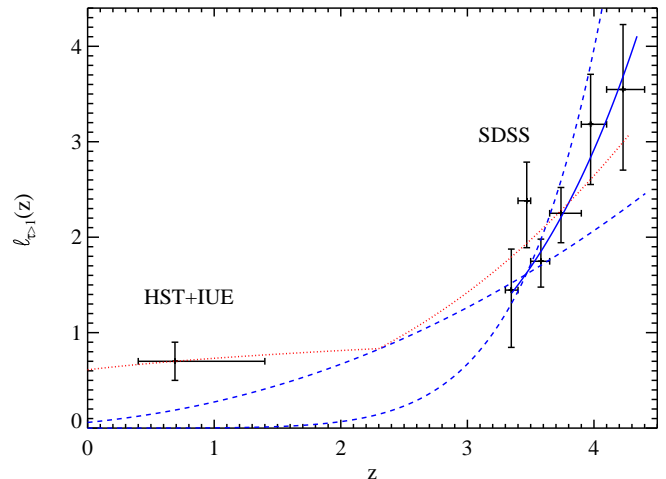


FIG. 15.— A comparison of our results from the SDSS-DR7 survey of LLSs (scaled to $\tau_{912} \geq 1$) against the $z < 1$ results from Stengler-Larrea et al. (1995). The (blue) solid and dashed curves show the best-fit to the SDSS observations and $\pm 2\sigma$ deviations from that fit. None of the curves, when extrapolated to $z = 0$, intersect the low z observations. We rule out at high confidence that a single power-law $(1+z)^{\gamma_{\text{LLS}}}$ is a good description of the observations from $z = 0-4$. Instead, we suggest a break at $z \approx 2$, here modeled (dotted, red line) as two power-laws with $\gamma_{\text{LLS}} = 2.78$ for $z > 2.3$ and $\gamma_{\text{LLS}} = 0.26$ otherwise.

$z = 0-4$. Instead, the data suggest a ‘break’ in the high z power-law at $z \sim 2$, similar to that observed for the Ly α forest although at somewhat higher redshift.

The dotted curve, is an attempt to model this break. For $z < 2.3$, we adopt the power-law form that matches the Ly α forest at low redshift ($\gamma_{\text{LLS}} = 0.26$) and demand that it intersect the central value of the Stengler-Larrea et al. (1995) measurement. For $z \geq 2.3$, the model breaks to a $\gamma_{\text{LLS}} = 2.78$ power-law, again consistent with the high z evolution of the Ly α forest (e.g. Kim et al. 2002). This is a reasonably good description of the data and we conclude that a break in the power-law description of $\ell_{\tau \geq 1}(z)$ likely occurs at $z \approx 2$. We will test this prediction with an (ongoing) survey for LLSs at $z \sim 2$ in HST/ACS and WFC3 slitless spectra of $z \approx 2.3$ quasars (PI: O’Meara).

9.3. The Average LLS Spectrum

To gain additional insight into the absorption properties of the LLSs, we have constructed an average (stacked) spectrum by (i) shifting each quasar spectrum containing a $\tau_{912} \geq 2$ LLSs to its rest-frame (192 systems total) and (ii) averaging the fluxed data. This stacked spectrum is primarily illustrative; it is shown in Figure 16. The peak in emission at $\lambda \approx 1280\text{\AA}$ is from the Ly α emission peak of the background quasars. The peak is offset from 1215\AA because the stack only includes intervening LLSs, i.e. those that are offset by at least 3000 km s^{-1} from the quasar emission redshift. The peak’s proximity to 1215\AA and relatively narrow width, however, reflect that most LLSs in our survey are located within $\delta z = 0.2$ of the quasar emission redshift.

The second strongest feature in the spectrum is the Lyman limit at the expected wavelength of 912\AA . Shortward of the Lyman limit, one observes a non-zero flux that extends down to $\approx 770\text{\AA}$. We estimate the average optical depth of the Lyman limit absorption in this

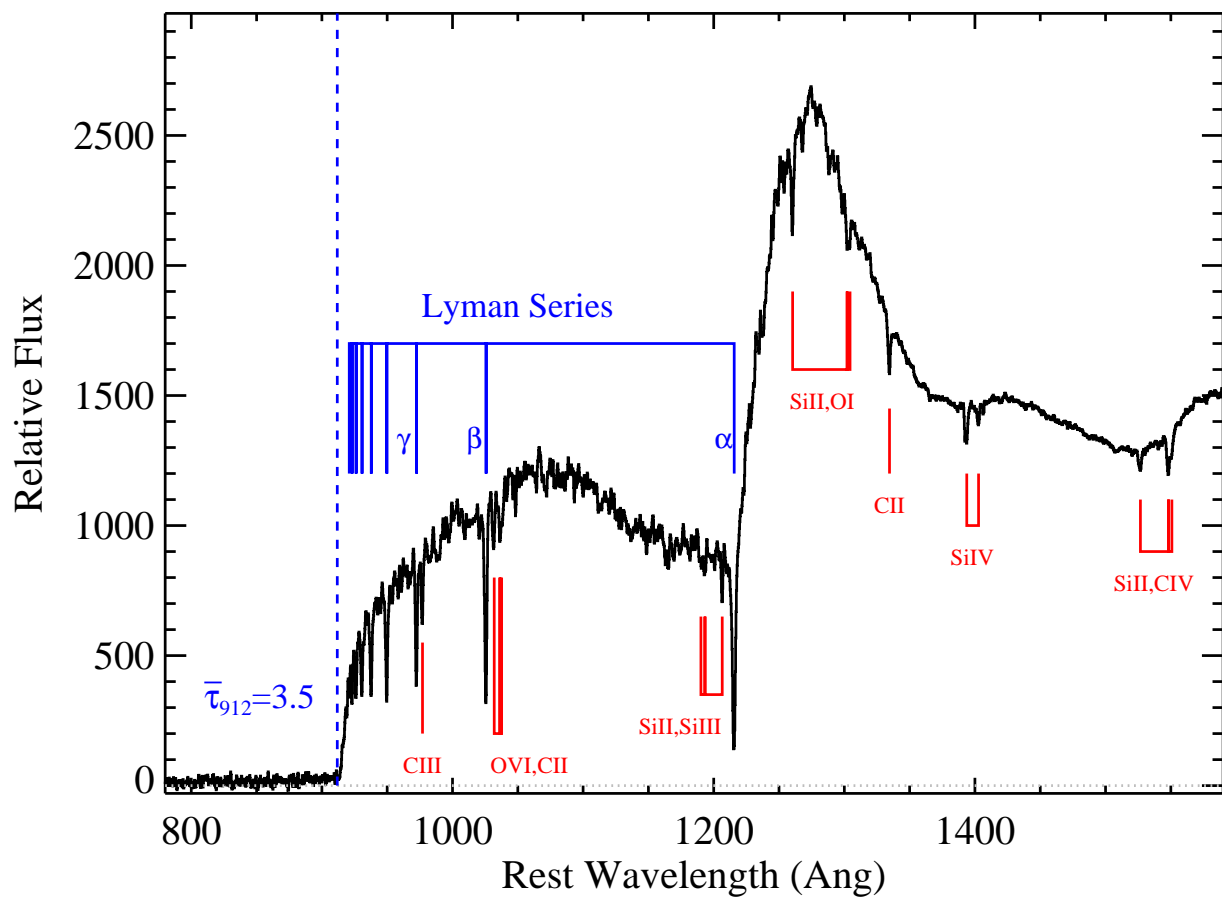


FIG. 16.— The average absorption spectrum of $\tau_{912} \geq 2$ LLSs at $z \approx 3.7$. Absorption from the H I Lyman series is readily apparent and one also notes strong Lyman limit absorption, as marked by the dashed vertical line. The measured average optical depth at the Lyman limit is $\bar{\tau}_{912} \approx 3.5$, a value that is inconsistent (too low) with our derived $f(N_{\text{HI}}, X)$ distribution. We infer that the stack includes the contribution from a small, but non-negligible number of LLSs having $\tau_{912} < 2$. The figure also identifies a series of metal-line transitions arising from low and high-ions. The presence of strong O VI absorption is especially notable and suggests that LLSs are comprised of gas in multiple phases.

stacked spectrum by assuming the flux at 980\AA provides a rough estimate of the absorbed continuum at the Lyman limit and measure

$$\bar{\tau}_{912} = -\ln \left[\frac{f(900\text{\AA})}{f(980\text{\AA})} \right] = 3.5 \quad (24)$$

We estimate a 20% error in this value due to effects related to sky subtraction, uncertainty in the absorbed continuum $f(980\text{\AA})$, and the flux-weighted average of our stack.

The value of $\bar{\tau}_{912}$ may be compared to the average optical depth derived from our $f(N_{\text{HI}}, X)$ distribution:

$$\bar{\tau}_{912} = -\ln \left\{ \frac{\int \exp[-N_{\text{HI}}\sigma_{\text{LL}}] f(N_{\text{HI}}, X) dN_{\text{HI}}}{\int f(N_{\text{HI}}, X) dN_{\text{HI}}} \right\} \quad (25)$$

where the integrals are evaluated over the interval $N_{\text{HI}} = [10^{17.5}, 10^{22}] \text{cm}^{-2}$. Evaluating at $z = 3.7$ using the $f(N_{\text{HI}}, X)$ distribution function shown in Figure 10, we derive $\bar{\tau}_{912} \approx 5.4$. The frequency distribution in the LLS regime is sufficiently flat that the higher N_{HI} systems (SLLS, DLAs) contribute significantly to the average.

The offset between these two evaluations is most likely due to the inclusion of a non-negligible number of sys-

tems having $\tau_{912} < 2$. Our analysis of mock spectra and our internal comparison of the τ_{912} estimates for the LLS indicate that this occurs frequently. As described in § 5, we estimate a 0.2dex uncertainty in the N_{HI} values of LLSs with $\tau_{912} \approx 2$. Although our tests also suggest this does not significantly affect the estimate of $\ell_{\tau > 2}(z)$, it can have a significant effect on the $\bar{\tau}_{912}$ value in the stacked spectrum. We have repeated our calculation of $\bar{\tau}_{912}$ extending the lower limit of the N_{HI} distribution to $N_{\text{HI}} = 10^{17.2} \text{cm}^{-2}$ instead of $N_{\text{HI}} = 10^{17.5} \text{cm}^{-2}$. For our favored $f(N_{\text{HI}}, X)$ distribution, we calculate $\bar{\tau}_{912} = 4.1$ and when allowing for sample variance with a bootstrap analysis we find consistency in a non-negligible fraction of the trials ($> 5\%$).

Returning to the stacked spectrum (Figure 16), we note a series of absorption lines corresponding to strong metal-line transitions of low and high ionization ions. This suggests a highly ionized, and possibly multi-phase gas. The strong absorption of O VI, in particular, suggests a multi-phase medium consisting of at least one “cool” ($T \approx 10^4\text{K}$), photoionized phase and another, more highly ionized phase which is presumably “warmer” ($T \gtrsim 10^5\text{K}$) and possibly collisionally ionized. This highly ionized phase has been detected in the damped Ly α systems (Wolfe & Prochaska 2000; Fox et al. 2007a)

and SLLSs (Fox et al. 2007b) and its presence in our average spectrum suggests it likely exists in lower N_{HI} systems too (e.g. Simcoe et al. 2004). A more quantitative analysis of the metal-line absorption in LLSs, however, awaits high-resolution spectroscopy (e.g. Prochter et al. 2009).

9.4. The Physical Nature of the LLSs

As described in the introduction, observations and numerical simulations associate the DLAs with high z galaxies residing in virialized dark matter halos (e.g. Møller et al. 2002; Pontzen et al. 2008). The majority of absorption lines comprising the Ly α forest, meanwhile, are believed to trace Mpc-scale overdensities in the medium between such galaxies (e.g. Miralda-Escudé et al. 1996). By inference, one may associate LLSs with lower N_{HI} ($< 10^{20} \text{ cm}^{-2}$) with the interface between the IGM and galaxies. This inference, however, has not yet been extensively tested by cosmological simulations or empirical observation. Early works on the topic generally yielded too few LLSs in cosmological volumes (Katz et al. 1996; Gardner et al. 2001; Maller et al. 2003). More recently, Kohler & Gnedin (2007) examined LLSs in a suite of simulations tuned to match the observed incidence of LLSs at $z \sim 4$. Their simulations suggest LLSs are highly ionized gas occupying volumes of space with dimension 1 – 100 kpc and physically associated with galaxies of a wide range in mass. The simulations, however, were not rigorously tested against observations nor did they have sufficient spatial resolution to “establish the physical nature of these systems”. The question remains: what is the physical nature of the LLSs?

Our observations place new constraints on the structures that give rise to LLSs absorption. The most informative measurements are $\ell_{\tau \geq 2}(X)$ and the shape of $f(N_{\text{HI}}, X)$ in the LLSs regime. Consider first $\ell_{\tau \geq 2}(X)$, which is proportional to the comoving number density n_{LLS} of the structures times their average physical size σ_{LLS} . In Figure 9, we present the $\ell(X)$ values (in cumulative form) for DLAs (Prochaska & Wolfe 2009) and SLLSs (O’Meara et al. 2007). For the latter, we assume $\ell_{\text{SLLS}}(X) = 0.20$ at all redshifts. We have adopted a 20% lower (1σ) value than reported by O’Meara et al. (2007) to crudely correct for the SDSS quasar targeting bias that will affect their measurement (PWO09). The figure demonstrates that the DLAs (especially) and the SLLSs have modest contributions to $\ell_{\tau \geq 2}(X)$. At $z = 3.4$, they contribute roughly half of the observed incidence of $\tau_{912} \geq 2$ LLS decreasing to $\approx 33\%$ by $z = 4$. This latter conclusion hinges on our assumptions for $\ell_{\text{SLLS}}(X)$, in particular at $z \approx 4$ where the value is not well constrained, but we expect the SLLSs to behave similarly to the DLAs whose incidence is not increasing significantly at these redshifts. We conclude that the incidence of $\tau_{912} \lesssim 10$ LLSs $\ell_{\text{LLS}}(z)$ is comparable to that of the DLAs and SLLSs. As a result, it is reasonable to associate all LLSs with the same structures, i.e. gas within virialized halos as suggested by Kohler & Gnedin (2007). The principle challenge to this association is whether diffuse halo gas has sufficiently high cross-section to LLS absorption. In particular, one should consider whether the “cold-flows” identified in numerical simulations of galaxy formation (Kereš et al. 2005; Dekel et al. 2009) have sufficient density and size to explain the majority of LLSs.

We are currently pursuing such analysis.

Now consider the evolution in $\ell_{\tau \geq 2}(X)$ with redshift. As noted in § 8.2, $\ell_{\tau \geq 2}(X)$ is observed to decrease with decreasing redshift. Examining Figure 9 it is evident that this decrease is driven by LLS with lower τ_{912} , i.e. by a significant decrease in $\ell_{\text{LLS}}(X)$. One possible explanation for this decrease would be an increase in the intensity of the EUVB with decreasing redshift, most likely due to higher emissivity from the quasar population. Unlike the DLAs and SLLSs systems which have $\tau_{912} > 100$ and therefore have regions that are self-shielded from the EUVB, the $\tau_{912} \lesssim 10$ LLSs are probably highly ionized throughout (e.g. Prochter et al. 2009). Similar to the Ly α forest, the $\tau_{912} \lesssim 10$ LLSs are sensitive to changes in the EUVB. This interpretation would predict that the average U parameter for $\tau_{912} \lesssim 10$ LLSs increase with decreasing redshift. Another possible interpretation arises from linking LLS absorption to the cold-flows in galactic halos predicted by numerical simulations. The simulations reveal that the incidence of cold-flows in massive halos $M \gtrsim 10^{12} M_{\odot}$ decreases with redshift Dekel et al. (2009), which could result in a lower $\ell_{\tau \geq 2}(X)$ for the LLSs. These assertions warrant further study and are likely to impact our understanding of the evolution in the mean free path of the universe (PWO09).

Finally, consider the constraints on $f_{\text{LLS}}(N_{\text{HI}}, X)$ set by the observations. As described in Figure 10, we find that $f(N_{\text{HI}}, X)$ flattens at $N_{\text{HI}} < 10^{19} \text{ cm}^{-2}$ to a power-law shallower than $\beta \approx -1$. The direct implication is that the cross-section of gas with $N_{\text{HI}} = 10^{19} \text{ cm}^{-2}$ exceeds that of gas with $N_{\text{HI}} = 10^{17.5} \text{ cm}^{-2}$. This is a remarkable result. Collapsed structures are generally observed to have a density gradient where the highest density regions occupy a smaller projected cross-section than lower density regions. Our observations indicate the opposite is true for LLSs with $\tau_{912} \lesssim 10$. This suggests that LLSs arise in structures with an extended, higher surface density region surrounded by a thin ‘layer’ of gas with lower N_{HI} . Such a description brings to mind the cold-flows of accreting gas found in cosmological simulations of high z galaxies (Kereš et al. 2005; Dekel et al. 2009). Again, we plan to explore whether such gas can explain the observed normalization and shape of $f(N_{\text{HI}}, X)$ at $z > 3.5$.

10. SUMMARY

In this paper, we have performed a survey for $\tau_{912} \geq 2$ LLS absorption in the quasar spectra of the Sloan Digital Sky Survey, Data Release 7. We established a spectral sample for statistical analysis (§ 3), estimated an absorbed continuum for each quasar (§ 4), searched for LLSs using automated algorithms (§ 5), defined the survey path with strict criteria (§ 6), and explored the effects of systematic bias and uncertainty with mock spectra (§ 7). The primary results of this work are as follows:

1. We measure the incidence of $\tau_{912} \geq 2$ LLSs $\ell_{\tau \geq 2}(z)$ at $z = 3.3 - 4.4$ and find it is well modeled as a single power-law, $\ell_{\tau \geq 2}(z) = C_{\text{LLS}}[(1+z)/(1+z_*)]^{\gamma_{\text{LLS}}}$, with $z_* \equiv 3.7$, $C_{\text{LLS}} = 1.9 \pm 0.2$, and $\gamma_{\text{LLS}} = 5.2 \pm 1.5$ (68% c.l.).
2. A survey of LLSs in the SDSS spectra $z_{\text{em}} < 3.6$ quasars confirms a previously identified bias

(PWO09) in the SDSS quasar targeting criteria that biases the sample toward sightlines with foreground LLS absorption.

3. The number of $\tau_{912} \geq 2$ LLS per unit absorption length $\ell_{\tau \geq 2}(X)$ is observed to decrease by $\approx 50\%$ from $z = 4$ to 3.4. This indicates a decrease in the number of systems per comoving Mpc^3 and/or a decrease in the average physical cross-section per system. We suggest it is the latter effect, possibly related to an increase in the EUVB with decreasing redshift or a rising radiation field local to LLSs.
4. The measured $\ell_{\tau \geq 2}(X)$ values place an integral constraint on the H I frequency distribution $f(N_{\text{HI}}, X)$ at $z \approx 3.7$. Adopting previous estimates of $f(N_{\text{HI}}, X)$ for $N_{\text{HI}} \geq 10^{19} \text{ cm}^{-2}$ (O’Meara et al. 2007; Prochaska & Wolfe 2009), we constrain $f(N_{\text{HI}}, X)$ for $N_{\text{HI}} = 10^{17.5} - 10^{19} \text{ cm}^{-2}$ assuming a power-law form $f_{\text{LLS}}(N_{\text{HI}}, X) = k_{\text{LLS}} N_{\text{HI}}^{\beta_{\text{LLS}}}$ to have $k_{\text{LLS}} \approx 10^{-4.5}$ and $\beta_{\text{LLS}} = -0.8 \pm 0.3$. This indicates a further shallowing of the slope as one decreases N_{HI} below 10^{19} cm^{-2} .
5. Adopting constraints from the mean free path (PWO09) and Ly α forest, we derived new constraints on $f(N_{\text{HI}}, X)$ at $z \approx 3.7$ for $N_{\text{HI}} \approx 10^{15} - 10^{18} \text{ cm}^{-2}$. We find that $\beta \equiv d \ln f(N_{\text{HI}}, X) / d \ln N_{\text{HI}}$ must be steeper than $\beta = -1.5$ at $N_{\text{HI}} \approx 10^{15} \text{ cm}^{-2}$.
6. We surveyed the spectra for proximate LLSs (PLLSs), those with redshifts that are within 3000 km s^{-1} of the quasar. We measure an $\approx 25\%$ lower incidence of PLLSs than intervening systems at $z > 3.5$. This lends further support to the assertion that quasars have anisotropic emission (Henawi & Prochaska 2007).

Compared to previous work, our estimates of $\ell(z)$ show systematically lower values. We suggest that the difference is due to sample variance and/or unidentified systematic bias in the prior analysis. This conclusion is supported by measurements of the mean free path (PWO09) which do not allow for a significantly higher incidence of LLSs. We also find that the range of power-laws that describe our results at $z \approx 3.5 - 4$ do not extrapolate to the results from $z < 1$ observations (Stengler-Larrea et al. 1995). We infer that the incidence of LLSs exhibits a break at $z \approx 2$, qualitatively similar to that observed for the Ly α forest (e.g. Weymann et al. 1998). The declining incidence of LLSs per absorption length and the very shallow slope of $f(N_{\text{HI}}, X)$ at $N_{\text{HI}} < 10^{19} \text{ cm}^{-2}$ suggest that $\tau_{912} \lesssim 10$ LLSs arise in flattened (e.g. filamentary) structures that have relatively sharp edges. We associate these structures to the virialized halos that presumably give rise to SLLS and DLA absorption. Finally, we encourage future work on whether such structures are con-

sistent with the “cold-flows” identified in numerical simulations.

Through detailed analysis of biases and careful sample selection from a large and homogeneous dataset, this paper provides the first robust estimate of the incidence of LLSs at high redshift. We note that the systematic errors described in § 7 likely limit the precision of any future $\ell(z)$ estimates to the order of 20–30%. Nevertheless, this is sufficient to further explore the true evolution in $\ell(z)$ with redshift. Programs with the Hubble Space Telescope for absorption at $z < 2$ and with ground-based observatories for $z > 4$ are currently ongoing. Altogether, these projects will describe the evolution of the UV background, the growth of structure on galactic (and larger) scales, and the chemical enrichment history of the universe.

The authors wish to recognize and acknowledge the very significant cultural role and reverence that the summit of Mauna Kea has always had within the indigenous Hawaiian community. We are most fortunate to have the opportunity to conduct observations from this mountain. We thank P. Madau, M. Fumagalli, and C. Faucher-Giguere for helpful comments. This work was initiated in collaboration with S. Burles. J. X. P. and J.M.O. are supported by NASA grants HST-GO-10878.05-A and HST-GO-11594.01. J.X.P. and G.W. are partially supported by an NSF CAREER grant (AST-0548180) and by NSF grant AST-0908910.

Funding for the SDSS and SDSS-II has been provided by the Alfred P. Sloan Foundation, the Participating Institutions, the National Science Foundation, the U.S. Department of Energy, the National Aeronautics and Space Administration, the Japanese Monbukagakusho, the Max Planck Society, and the Higher Education Funding Council for England. The SDSS Web Site is <http://www.sdss.org/>.

The SDSS is managed by the Astrophysical Research Consortium for the Participating Institutions. The Participating Institutions are the American Museum of Natural History, Astrophysical Institute Potsdam, University of Basel, University of Cambridge, Case Western Reserve University, University of Chicago, Drexel University, Fermilab, the Institute for Advanced Study, the Japan Participation Group, Johns Hopkins University, the Joint Institute for Nuclear Astrophysics, the Kavli Institute for Particle Astrophysics and Cosmology, the Korean Scientist Group, the Chinese Academy of Sciences (LAMOST), Los Alamos National Laboratory, the Max-Planck-Institute for Astronomy (MPIA), the Max-Planck-Institute for Astrophysics (MPA), New Mexico State University, Ohio State University, University of Pittsburgh, University of Portsmouth, Princeton University, the United States Naval Observatory, and the University of Washington.

APPENDIX

COMPARISONS WITH KECK+LRIS SPECTRA

To assess uncertainties (statistical and systematic) of surveying LLSs in the SDSS quasar spectra, we obtained independent, higher quality spectra using the LRIS spectrometer (Oke et al. 1995) on the Keck I telescope. LRIS employs a dichroic to split the data into two spectral channels, each with its own camera. For our observations, we

employed the d560 dichroic which splits the light at $\approx 5600\text{\AA}$. For the blue channel, we used the 640/4000 grism which provides a dispersion of 0.63\AA per unbinned pixel and has a nominal wavelength coverage of $3100\text{\AA} < \lambda < 5600\text{\AA}$. The blue channel data was binned by 2 in both the spatial and spectral dimensions. For the red channel, we used the 600/7500 grating which provides a dispersion of 1.28\AA per unbinned pixel, and which was tilted to provide a wavelength coverage of $5600\text{\AA} < \lambda < 8200\text{\AA}$. The red channel data was unbinned. All observations were obtained using a 1 arc-second slit which provides an ≈ 4 pixel FWHM corresponding to $\approx 290\text{km s}^{-1}$ and $\approx 220\text{km s}^{-1}$ for the blue and red data respectively. The data were obtained in good sky conditions during a 4 night run in October 2008 and had exposure times ranging from 300 to 500 seconds. The data were reduced using the LowRedux pipeline¹² which bias subtracts, flat fields, optimally extracts, wavelength and flux calibrates the data to produce a final 1D spectrum.

The SDSS targets for LRIS observations were chosen to sample a range of LLSs, e.g., LLSs with $\tau_{912} \geq 2$, pLLSs candidates, PLLSs and spectra without apparent LLSs. Furthermore, an emphasis was placed on quasars with lower S/N SDSS spectra to assess the completeness of recovering LLSs. In all cases, the LRIS spectra have sufficient S/N to unambiguously detect the presence of absorbers with $\tau_{912} > 1$ over the full SDSS wavelength range (i.e. $\lambda > 3800\text{\AA}$) for the intervening LLS survey. Particular emphasis was given to determine what absorbed continuum S/N cutoff should be applied to the SDSS sample. To this end, two of the authors (JXP and JMO) independently modeled LLS absorption in the LRIS data and compared the results to similar analysis of the the SDSS spectra. The same codes were used to model LLS absorption. In Table A1, we present the results of these comparisons. In Figure A1 we show a representative sample of the LRIS data alongside their SDSS counterparts. For the SDSS data in Figure A1, we also show the continuum level assigned to each spectrum.

The LRIS/SDSS comparison illustrates that with a choice of absorbed continuum S/N > 1 we recover nearly 100% of the LLSs with $\tau_{912} > 2$ in the SDSS. We see this explicitly in Table A1, where we give the values for z_{start} in the SDSS search, where z_{start} is the redshift at which the absorbed continuum S/N crosses the value of 1. In some cases, we identify LLSs at redshifts lower than z_{start} in both the LRIS and SDSS data. Although these LLSs will not contribute to our results, they lend additional confidence in our absorbed continuum S/N cutoff. The only exceptions to the identification of LLSs in the LRIS and SDSS spectra at S/N ≥ 1 are for systems with $\tau_{912} \approx 2$. At this optical depth, JXP and JMO did not always agree, even in the LRIS results. This highlights the fact that our results have an inherent uncertainty in $\log N_{\text{HI}}$ of ≈ 0.2 dex. Most importantly, this disagreement does not appear to depend on the S/N of the spectrum for the range of S/N we could expect from the SDSS data, and thus does not effect our choice for the S/N threshold.

REFERENCES

- Abazajian, K. N., et al. 2009, *ApJS*, 182, 543
Bahcall, J. N., & Peebles, P. J. E. 1969, *ApJ*, 156, L7+
Croft, R. A. C., Weinberg, D. H., Bolte, M., Burles, S., Hernquist, L., Katz, N., Kirkman, D., & Tytler, D. 2002, *ApJ*, 581, 20
Dall’Aglio, A., Wisotzki, L., & Worseck, G. 2008, *A&A*, 491, 465
Davé, R., Hernquist, L., Katz, N., & Weinberg, D. H. 1999, *ApJ*, 511, 521
Dekel, A., et al. 2009, *Nature*, 457, 451
Faucher-Giguère, C., Lidz, A., Zaldarriaga, M., & Hernquist, L. 2009, *ArXiv e-prints*
Faucher-Giguère, C.-A., Lidz, A., Hernquist, L., & Zaldarriaga, M. 2008a, *ApJ*, 688, 85
Faucher-Giguère, C.-A., Prochaska, J. X., Lidz, A., Hernquist, L., & Zaldarriaga, M. 2008b, *ApJ*, 681, 831
Fox, A. J., Petitjean, P., Ledoux, C., & Srianand, R. 2007a, *A&A*, 465, 171
—, 2007b, *ApJ*, 668, L15
Gardner, J. P., Katz, N., Hernquist, L., & Weinberg, D. H. 2001, *ApJ*, 559, 131
Guimaraes, R., Petitjean, P., Ramos De Carvalho, R., Djorgovski, G., Noterdaeme, P., Castro, S., Da Rocha Poppe, P., & Aghaee, A. 2009, *ArXiv e-prints*
Hennawi, J. F., & Prochaska, J. X. 2007, *ApJ*, 655, 735
Herbert-Fort, S., Prochaska, J. X., Dessauges-Zavadsky, M., Ellison, S. L., Howk, J. C., Wolfe, A. M., & Prochter, G. E. 2006, *PASP*, 118, 1077
Hu, E. M., Kim, T.-S., Cowie, L. L., Songaila, A., & Rauch, M. 1995, *AJ*, 110, 1526
Hui, L., & Rutledge, R. E. 1999, *ApJ*, 517, 541
Katz, N., Weinberg, D. H., Hernquist, L., & Miralda-Escude, J. 1996, *ApJ*, 457, L57+
Kereš, D., Katz, N., Weinberg, D. H., & Davé, R. 2005, *MNRAS*, 363, 2
Kim, T., Cristiani, S., & D’Odorico, S. 2001, *A&A*, 373, 757
Kim, T.-S., Carswell, R. F., Cristiani, S., D’Odorico, S., & Giallongo, E. 2002, *MNRAS*, 335, 555
Kohler, K., & Gnedin, N. Y. 2007, *ApJ*, 655, 685
Lanzetta, K. M. 1991, *ApJ*, 375, 1
Madau, P., Haardt, F., & Rees, M. J. 1999, *ApJ*, 514, 648
Maller, A. H., Prochaska, J. X., Somerville, R. S., & Primack, J. R. 2003, *MNRAS*, 343, 268
McDonald, P., et al. 2005, *ApJ*, 635, 761
Meiksin, A., & Madau, P. 1993, *ApJ*, 412, 34
Miralda-Escudé, J., Cen, R., Ostriker, J. P., & Rauch, M. 1996, *ApJ*, 471, 582
Misawa, T., Tytler, D., Iye, M., Kirkman, D., Suzuki, N., Lubin, D., & Kashikawa, N. 2007, *AJ*, 134, 1634
Møller, P., Warren, S. J., Fall, S. M., Fynbo, J. U., & Jakobsen, P. 2002, *ApJ*, 574, 51
Noterdaeme, P., Petitjean, P., Ledoux, C., & Srianand, R. 2009, *A&A*, 505, 1087
Oke, J. B., et al. 1995, *PASP*, 107, 375
O’Meara, J. M., Prochaska, J. X., Burles, S., Prochter, G., Bernstein, R. A., & Burgess, K. M. 2007, *ApJ*, 656, 666
Péroux, C., Dessauges-Zavadsky, M., D’Odorico, S., Sun Kim, T., & McMahon, R. G. 2005, *MNRAS*, 363, 479
Péroux, C., McMahon, R. G., Storrie-Lombardi, L. J., & Irwin, M. J. 2003, *MNRAS*, 346, 1103
Petitjean, P., Webb, J. K., Rauch, M., Carswell, R. F., & Lanzetta, K. 1993, *MNRAS*, 262, 499
Pontzen, A., et al. 2008, *MNRAS*, 390, 1349
Prochaska, J. X. 1999, *ApJ*, 511, L71
Prochaska, J. X., Hennawi, J. F., & Herbert-Fort, S. 2008, *ApJ*, 675, 1002
Prochaska, J. X., Herbert-Fort, S., & Wolfe, A. M. 2005, *ApJ*, 635, 123
Prochaska, J. X., & Wolfe, A. M. 2009, *ApJ*, 696, 1543
Prochaska, J. X., Worseck, G., & O’Meara, J. M. 2009, *ApJ*, 705, L113
Prochter, G. E., Prochaska, J. X., Bernstein, R., & Burles, S. M. 2009, *ApJ*, in press
Rao, S. M., Turnshek, D. A., & Nestor, D. B. 2006, *ApJ*, 636, 610
Rauch, M. 1998, *ARA&A*, 36, 267
Richards, G. T., et al. 2002, *AJ*, 123, 2945
Russell, D. M., Ellison, S. L., & Benn, C. R. 2006, *MNRAS*, 367, 412

¹² <http://www.uchicago.edu/~xavier/LowRedux/>

TABLE A1
 SDSS-DR7 QUASARS WITH KECK+LRIS COMPARISON SPECTRA

Object Name	SDSS $z_{start,jxp}$	SDSS $z_{lls,jxp}$	SDSS $\log N_{HIjxp}$	SDSS $z_{start,jmo}$	SDSS $z_{lls,jmo}$	SDSS $\log N_{HIjmo}$	LRIS $z_{lls,jxp}$	LRIS $\log N_{HIjxp}$	LRIS $z_{lls,jmo}$	LRIS $\log N_{HIjmo}$
J000300+160028	3.594	3.570	17.2	3.643	3.621	17.2	3.493	17.4	3.611	17.0
J002946-093541	3.411	3.523	> 17.5	3.682	3.482	> 17.5	3.563	17.4	3.524	17.4
J004143-085705	3.302	3.605	> 17.5	3.650	3.616	17.4	3.606	> 17.5	3.605	> 17.5
J023923-081005	0.000	0.000	0.0	0.000	0.000	0.0	3.827	> 17.5	3.801	17.4
J024448-081606	0.000	0.000	0.0	3.280	3.957	17.2	3.949	17.4	3.980	17.4
J025105-001732	3.725	3.438	16.8	3.728	3.276	17.2	3.434	17.2	3.262	> 17.5
J170035+342109	0.000	0.000	0.0	0.000	0.000	0.0	3.064	> 17.5	3.061	> 17.5
J171422+314802	3.280	3.468	17.0	3.280	3.395	17.0	3.275	17.4	3.274	17.4
J171705+303931	3.280	3.480	> 17.5	3.280	3.475	> 17.5	3.476	> 17.5	3.477	> 17.5
J171800+621326	3.636	3.614	17.4	3.280	3.615	> 17.5	3.620	> 17.5	3.615	> 17.5
J173039+585847	0.000	0.000	0.0	0.000	0.000	0.0	2.776	> 17.5	2.775	> 17.5
J173115+563641	3.701	3.562	17.2	3.701	3.562	17.4	3.397	> 17.5	3.399	> 17.5
J204230-060112	0.000	0.000	0.0	0.000	0.000	0.0	3.862	17.4	3.863	> 17.5
J205142-071906	3.816	3.780	17.2	0.000	0.000	0.0	3.799	> 17.5	3.796	17.4
J205509-071749	0.000	0.000	0.0	3.280	3.859	> 17.5	3.553	> 17.5	3.550	> 17.5
J205551-004814	0.000	0.000	0.0	0.000	0.000	0.0	3.176	> 17.5	3.174	> 17.5
J210055-004843	3.538	3.331	> 17.5	3.597	3.357	> 17.5	3.331	> 17.5	3.329	> 17.5
J212204-001012	3.625	3.267	> 17.5	3.625	3.407	> 17.5	3.405	17.0	3.406	17.2
J212358-005350	3.280	3.626	> 17.5	3.280	3.627	> 17.5	3.626	> 17.5	3.626	> 17.5
J212444-005533	3.280	3.442	> 17.5	3.280	3.448	> 17.5	3.443	> 17.5	3.440	> 17.5
J214050+103832	3.754	3.737	17.2	3.760	3.745	17.2	3.705	17.2	3.687	17.2
J214227+005652	3.634	3.598	17.4	3.642	3.613	17.2	3.601	17.4	3.598	17.4
J220213-085222	3.280	0.000	0.0	3.280	0.000	0.0	3.144	> 17.5	3.143	> 17.5
J221014+114452	3.592	0.000	0.0	3.592	3.304	> 17.5	3.286	> 17.5	3.285	> 17.5
J221458+135345	3.509	3.480	17.2	3.510	3.486	16.6	3.167	17.4	3.449	17.2
J222420-085339	3.660	3.577	17.4	3.660	3.577	17.4	3.480	17.0	3.021	> 17.5
J222824+134155	3.280	0.000	0.0	3.302	3.944	16.8	3.725	17.2	3.442	17.0
J223659-080912	0.000	0.000	0.0	0.000	0.000	0.0	3.405	17.4	3.397	17.2
J224243-091544	0.000	0.000	0.0	4.182	4.162	17.2	4.108	17.4	4.113	17.2
J224740-091512	0.000	0.000	0.0	0.000	0.000	0.0	4.175	> 17.5	3.895	16.0
J225053-084600	3.513	3.716	17.0	3.735	3.720	17.0	3.299	> 17.5	3.300	> 17.5
J225109-083138	3.280	3.867	> 17.5	0.000	0.000	0.0	3.887	> 17.5	3.832	> 17.5
J225152+125707	3.547	3.386	17.2	3.547	3.386	17.4	3.360	> 17.5	3.360	> 17.5
J230022+125354	3.533	3.509	17.2	3.531	3.507	17.2	3.545	17.4	3.542	17.2
J230301-093931	3.280	3.316	> 17.5	3.280	3.312	> 17.5	3.311	> 17.5	3.308	> 17.5
J231137-084410	3.346	3.689	> 17.5	3.589	3.685	> 17.5	3.717	> 17.5	3.716	17.4
J232533+143247	0.000	0.000	0.0	3.665	3.647	17.4	3.551	> 17.5	3.554	17.4
J233535-085939	3.643	3.621	17.2	3.640	3.620	17.2	3.389	> 17.5	3.335	> 17.5
J233634+133043	0.000	0.000	0.0	0.000	0.000	0.0	3.110	> 17.5	3.215	17.4
J234349-104742	3.551	3.403	> 17.5	3.551	3.367	> 17.5	3.366	> 17.5	3.363	> 17.5

NOTE. — List of all objects which have LRIS comparison spectra

Sargent, W. L. W., Steidel, C. C., & Boksenberg, A. 1989, ApJS, 69, 703
 Shen, Y., et al. 2007, AJ, 133, 2222
 Simcoe, R. A., Sargent, W. L. W., & Rauch, M. 2004, ApJ, 606, 92
 Stengler-Larrea, E. A., et al. 1995, ApJ, 444, 64
 Storrie-Lombardi, L. J., McMahon, R. G., Irwin, M. J., & Hazard, C. 1994, ApJ, 427, L13
 Suzuki, N. 2006, ApJS, 163, 110
 Telfer, R. C., Zheng, W., Kriss, G. A., & Davidsen, A. F. 2002, ApJ, 565, 773
 Tytler, D. 1982, Nature, 298, 427

Tytler, D., et al. 2004, ApJ, 617, 1
 Weymann, R. J., et al. 1998, ApJ, 506, 1
 Wolfe, A. M., Gawiser, E., & Prochaska, J. X. 2005, ARA&A, 43, 861
 Wolfe, A. M., Lanzetta, K. M., Foltz, C. B., & Chaffee, F. H. 1995, ApJ, 454, 698
 Wolfe, A. M., & Prochaska, J. X. 2000, ApJ, 545, 591
 Worseck, G., & Prochaska, J. 2009, ApJ, submitted
 York, D. G., et al. 2000, AJ, 120, 1579
 Zuo, L. 1993, A&A, 278, 343

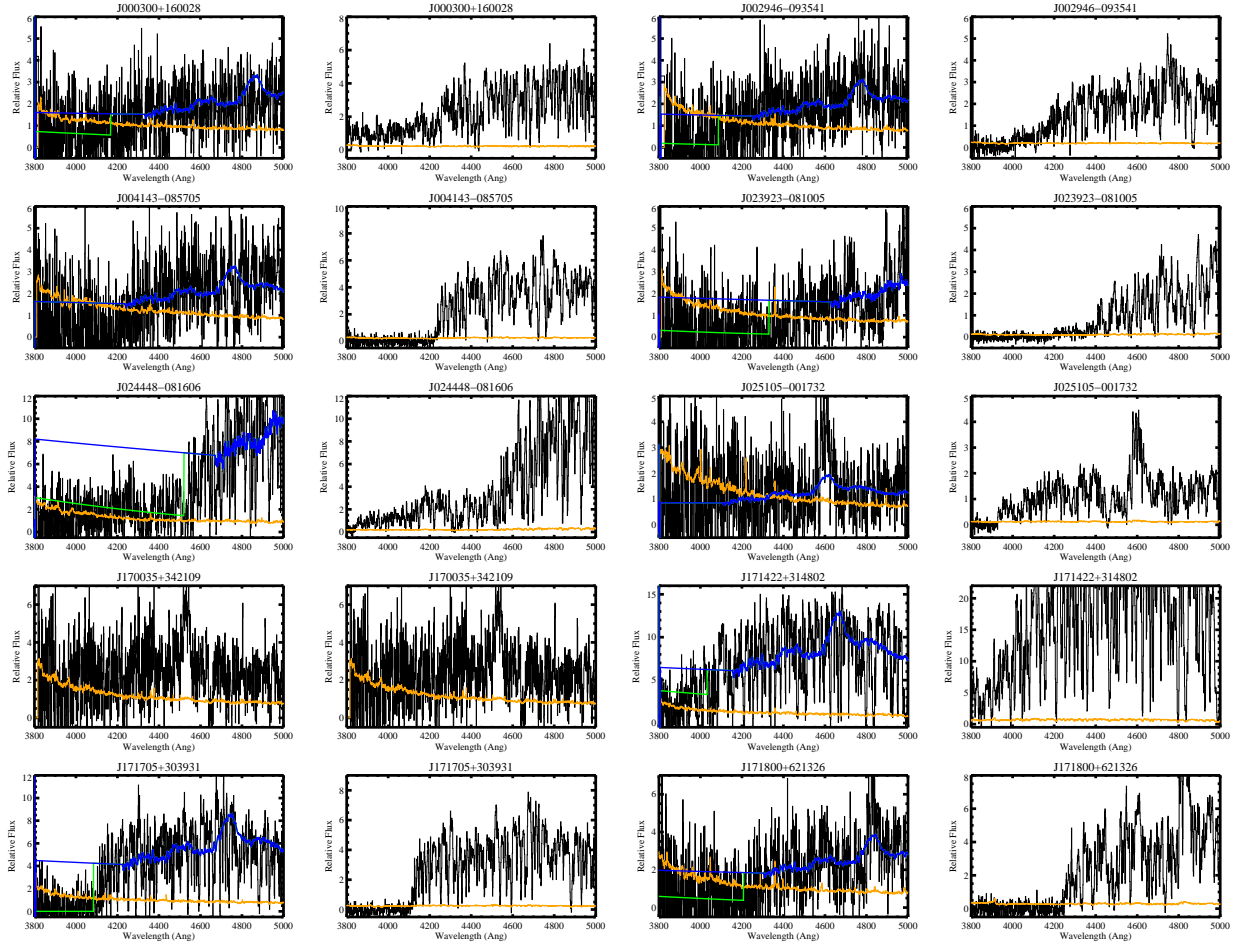


FIG. A1.— Comparisons of SDSS (left panel in each pair) and follow-up Keck/LRIS observations (right panel in each pair). Overplotted on the SDSS spectrum is our model of the absorbed continuum (blue) and the modeled foreground Lyman limit absorption (green). For the SDSS spectra with $S/N_{912}^{\text{Å}} \geq 2$, we find excellent agreement for analyses of each pair of spectra.